OBSERVATOIRE ROYAL
DE
BELGIQUE

KONINKLIJKE STERRENWACHT
VAN
BELGIE

GPS Report N° 16

GLOBAL OCEAN TIDES FROM INVERSION OF ALTIMETER AND TIDE GAUGE MEASUREMENTS

O. FRANCIS

Dec. 1992

Av. Circulaire 3 - 1180 Bruxelles
Ringlaan 3 - 1180 Brussel

Global ocean tides from inversion of altimeter and tide gauge measurements

Olivier FRANCIS

Progress Report

1992

Table of Contents

1. Introduction

The ultimate objective of the present work is to carry out an analysis of all the altimeter, tide gauge and gravity loading data in order to improve the knowledge of the global ocean tides. The tidal signal will be extracted by joint inversion of these three different kinds of data. The inverse method guarantees stability, unicity and optimality of the solution when all the available a priori informations of statistical character are taken into account. We have already computed inverse solutions of the global ocean tide for the principal semidiurnal tide M_2 by using : (a) only tide gauge data (Francis and Mazzega, 1991), (b) only gravity loading data (Francis and Mazzega, 1990a) and (c) all together tide gauge and gravity loading data (Jourdin et al., 1991). Point estimations of the ocean tides from altimetry have already been obtained by Mazzega and Jourdin (1991). Nevertheless, the results are somewhat insufficient essentially because the large scale errors are badly modelled. Our next goal is a global inverse solution from altimeter data. The innovation will be to solve globally the problem allowing the introduction of new constraints to separate the tidal signal from the errors. Particularly, the radial orbit error which has a long wave length behaviour should be better modelled at large scale as well as at small scale.

Inversion of altimeter data is a more difficult task than the inversion of the tide gauge or gravity loading data. Indeed, the budget of the altimeter measurements is complicated and the quantity of data delivered by the altimeter is huge. Today, it is unthinkable to process all the altimeter data together. In order to overcome this problem of amount of data, the altimeter data will be processed in two steps. Firstly, the long wave length phenomena like errors of the geoid and radial orbit error will be estimated by inversion of a reduced set of averaged altimeter data with a global coverage. Then, these estimated long wave length components will be subtracted from the complete set of altimeter data providing us with residues. In the second step, the smaller wave length phenomena like tides will be estimated from the residues with a dense and local set of altimeter data.

This report begin by a brief description of the satellite altimetry principle. The pre-processing and the reduction of the amount of altimeter data is then addressed. One chapter deals with results of a few spectral analyses of the Geosat altimeter data. Results of the complex demodulation of Geosat altimeter data are shown and will serve to correct the altimeter data themselves for the radial orbit errors. Finally, preliminary cotidal maps from inversion of Geosat altimeter data are presented and discussed with a view to further developments of the work.

2. Satellite Altimetry.

Working on the echo-sounder principle, the altimeter times the returns from compressed radar pulses transmitted vertically downward to the sea surface (Figure 1). After various instrumental, atmospheric and ionospheric corrections, the height of the mean sea surface is recovered to an accuracy of a few centimeters. The height of the sea surface with respect to the ellipsoid is deduced by subtracting the altimetric height (h_a) from the computed radial distance of the satellite (h_S). The orbital distance (h_S) is computed by specialized procedures involving mainly the earth's gravity field model and data from numerous tracking stations. Their accuracy is of the order of a meter at present in absolute terms (for GEOSAT with GEMT1 Gravity Potential).

In the following sections, the term altimeter data will represent the height of the ocean surface with respect to the geoid (h_d) i.e..the height of the ocean surface (h_S-h_a) with respect to the reference ellipsoid as determined by altimetry minus the geoid (h_g).

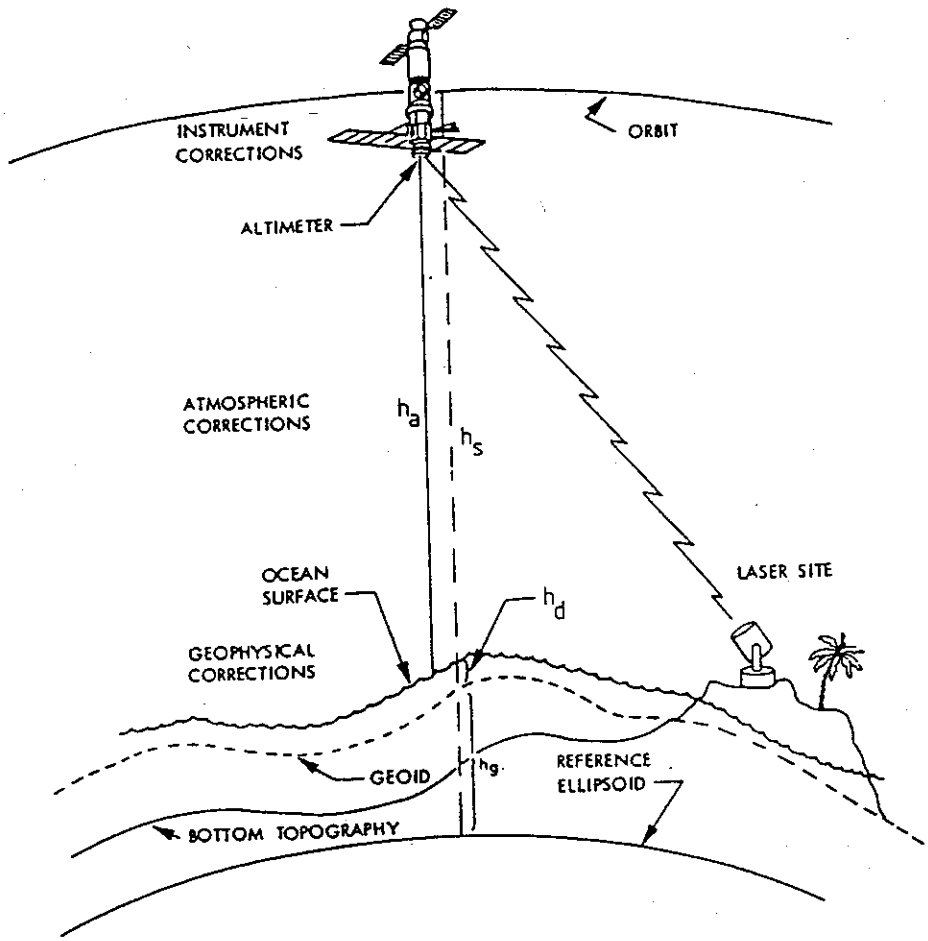

Figure 1: Principle of the satellite altimetry.

3. Pre-processing of the altimeter data

One year of GEOSAT altimeter data has been selected covering the period from the 8th November 1986 to the 18th November 1987. GEOSAT was an Exact Repeat Mission (ERM) with a repetitivity of about 17 days (say 1 cycle). So, the satellite flies over the same ground points every 17 days and one year contains 22 cycles.

The work which has been performed on the pre-processing of the altimeter data can be divided into two parts. The first one concerns validation and statistics on the raw data. The second part deals with the way of reducing the amount of data.

3.1 Raw altimeter data.

The basic file of Raw Altimeter Data (RAD) we use contains the Geosat data sampled every 3 seconds. These RAD corrected for environmental effects were prepared by Marty (1990). For the chosen year, there are about 5.3 10^6 data. The number of data considerably vary from one cycle to the other due to occasional malfunction of the altimeter.

The following processing has been applied on these RAD :

1. computation of the mean values of the RAD cycle by cycle (Figure 2)
2. drawings of the histogram of the RAD for each cycle : histogram of cycle 1 is given in Figure 3 as an example.
3. elimination of the outliers on the criterion :

if $|d^k_i - \langle d^k \rangle| > 3\ \sigma_k$ then d^k_i is eliminated

where d^k_i is the ith data of cycle k

$\langle d^k \rangle$ is the mean value of cycle k

σ_k is the standard deviation of cycle k

By using this criterion, about 84 10^3 data (i.e. 1.6 % of the total number of data) were eliminated.

4. elimination of the data above 66.94° North latitude and data below 66.95° South latitude.

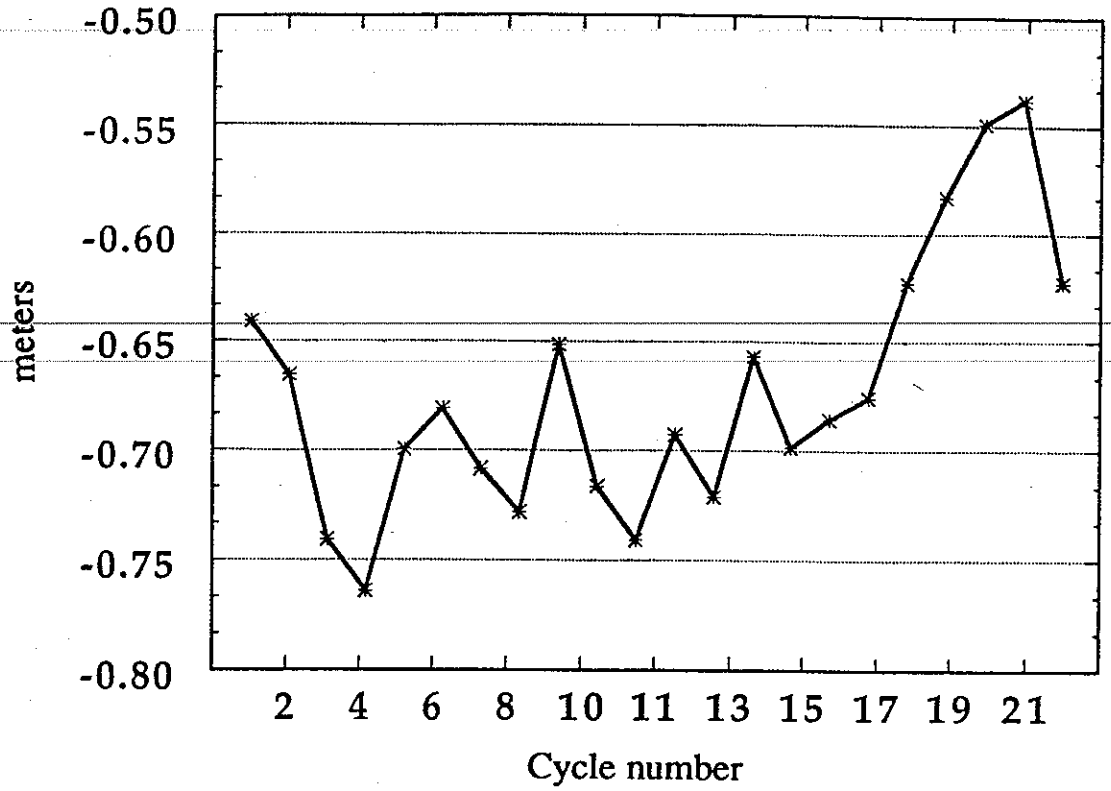

Figure 2 : Mean values (in meters) of the Raw Altimeter Data versus the cycle number.

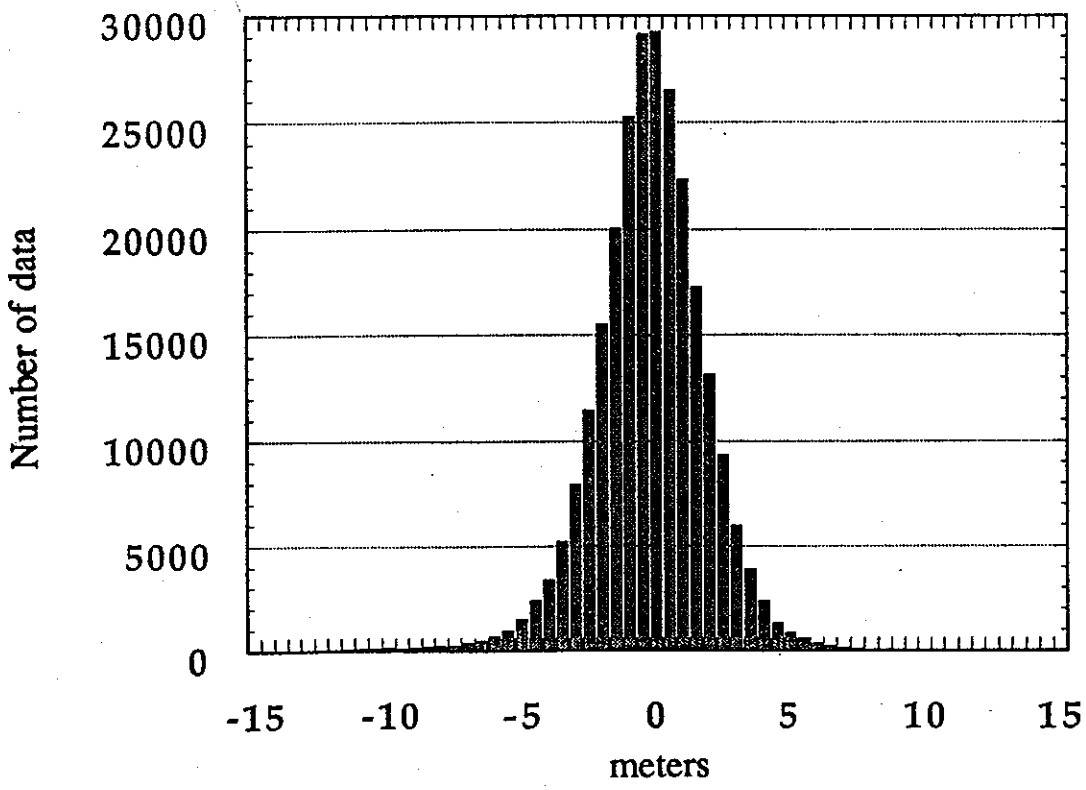

Figure 3 : Histogram of the Raw Altimeter Data of the cycle 1

3.2 Mean altimeter data

As explained in the introduction, the long wave length phenomena will be firstly estimated. This requires a global coverage of the altimeter data but not a dense sampling. So, the RAD have been averaged over 1 minute in order to reduce the number of data from $5.4\ 10^6$ to $259\ 10^3$. The mean have been performed in such a way that the Mean Altimeter Data (MAD) are lined up at the same latitudes 280 km apart (Figure 4). This spatial arrangement will be useful to the future data inversions. Indeed, the elements of the matrix to be inverted only depend upon the differential position of the data so that if one chooses the same data sampling for each cycle, the same matrix will be used for each cycle and ideally only one matrix inversion has to be computed.

For each cycle, there are 20,496 possible locations for the MAD including continental areas. The total number of locations sampled at least one time over the 22 cycles is 13,873 and there are 6,623 locations never sampled. This lack of data is largely due to the continental areas which cover about 6148 data positions. On the other hand, the total number of locations effectively sampled by all cycles is 5,506. Figure 5 shows the percentage of MAD locations sampled in function of the number of cycles. For instance, 40% of the MAD locations are sampled by the 22 cycles, 15% by 21 cycles, and so on...

Finally, the MAD have been formatted in a convenient way and recorded. A software allows a quick and efficient extraction of the MAD for future needs.

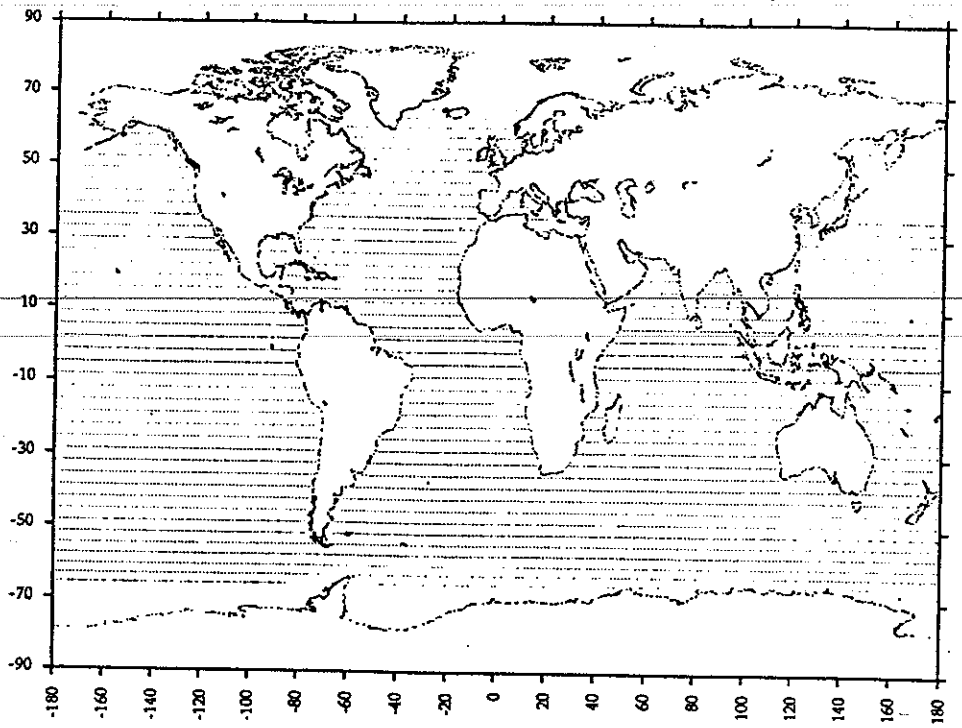

Figure 4 : Locations of the Mean Altimeter Data of the cycle 1.

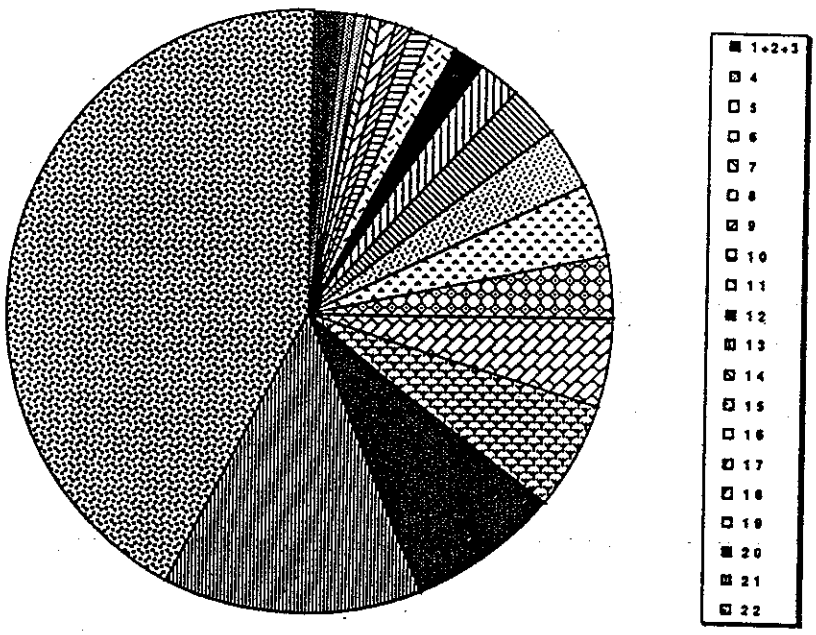

Figure 5 : Percentage of the Mean Altimeter Data locations sampled as function of the number of cycles.

4. Spectral analysis.

The MAD time series contain geophysical signals plus error signals. The geophysical signals consist of tides, permanent circulation, and so on. At this stage, we are more interested in the error components due to the error on the radial position of the satellite and on the errors of the geoid which is the reference surface of the altimeter data. Our goal is to find the best possible representation of these errors when geophysical signals, tides for instance, are extracted. Generally, the characterisation of the errors by their spectra is a very efficient mean. At first, we want to observe the spectral characteristics of the different components of the MAD. Subsequently, these characteristics will be theoretically derived and compared with the observed ones. Hence, the Fourier Transforms or spectra of the MAD time series have been computed. The well-known Fast Fourier Transform (FFT) which supposes equally spaced data could not be applied because the MAD are unequally distributed in-time on account of the continents where data are unavailable and of the failure of the altimeter. Therefore, a special routine (Laudet, 1988) for periodogram of unevenly sampled time series (Scargle, 1982) was used.

4.1 Fourier Transforms of the mean altimeter data

Figures 6 to 11 show the periodograms of the MAD for 6 typical cycles. A remarkable feature is the presence of the same periodicities in each cycles. Moreover, there is a dominant energetic peak in each cycle at 14,254 cycles per day which corresponds to 1 cycle per revolution of the satellite. All the other peaks appear at overtones 2, 3, 4,.. cycles per revolution. It is known that the signal at 1 cycle per revolution is largely due to the radial orbit error.

On the other hand, although the former similitude between the periodogram of the different cycles, there is a sensible variability of the amplitude of the main peaks from one cycle to the other. For example, the amplitude of the 1 cycle per revolution has values between 40 cm to 140 cm. This shows the non-stationarity of the signal (say probably the orbit error) at this frequency. This non-stationarity has been also observed inside the cycles themselves by making spectral analysis on periods of a half cycle.

Time series of the tidal height, of the height of the geoid (h_g in Figure 1) as well as of the height of the geoid plus the MAD were evaluated at the times and positions sampled during the cycle 1. There respective periodograms were computed (Figures 12 to 14). The tidal height has been computed by using a hydrodynamical model and its periodogram (Figure 12) shows the low amplitude and the complexity of the signal that

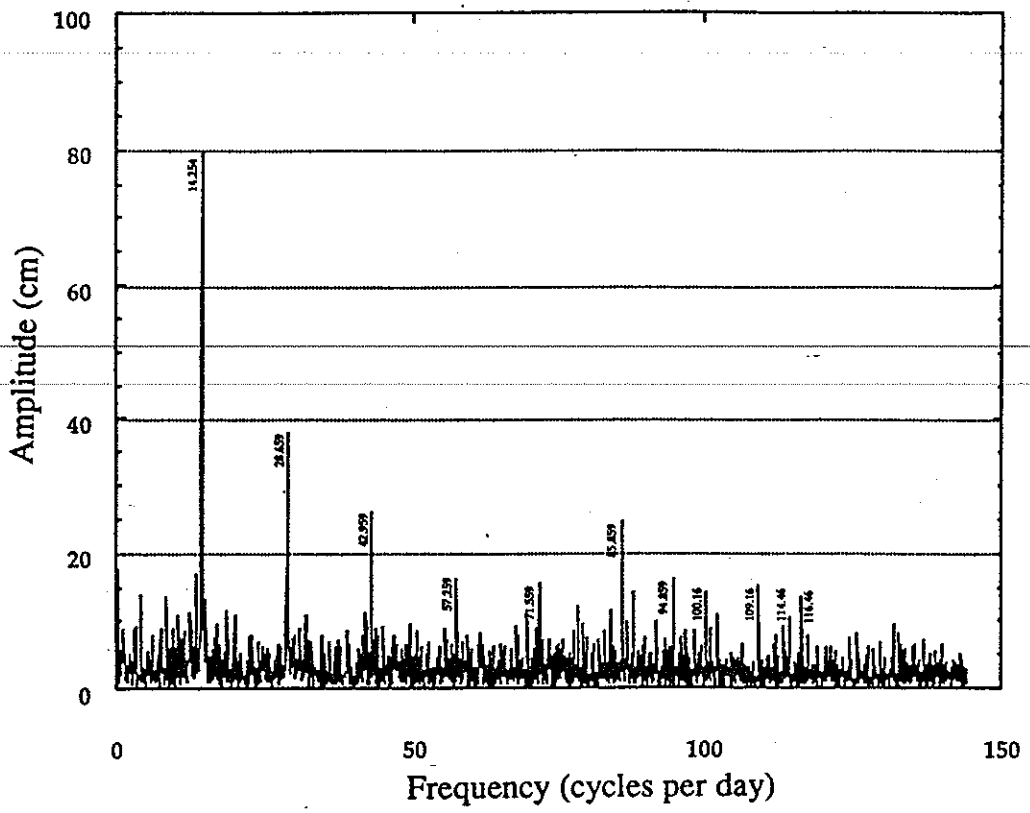

Figure 6 : Periodogram of the Mean Altimeter Data of the cycle 1.

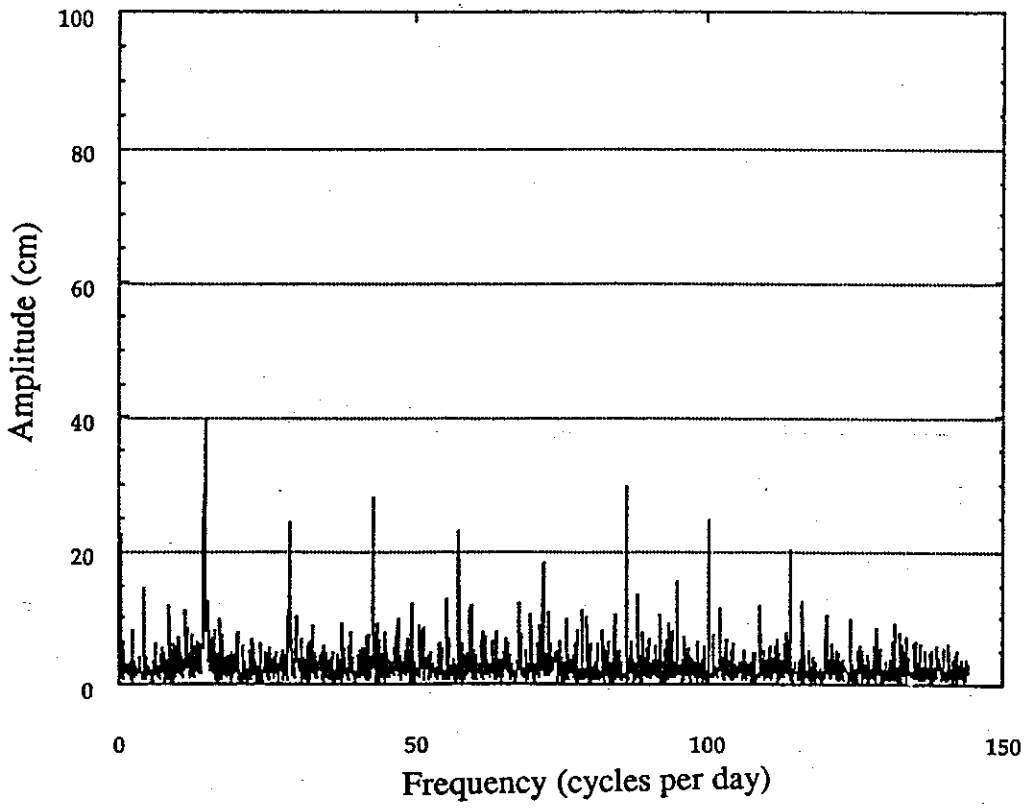

Figure 7 : Periodogram of the Mean Altimeter Data of the cycle 4.

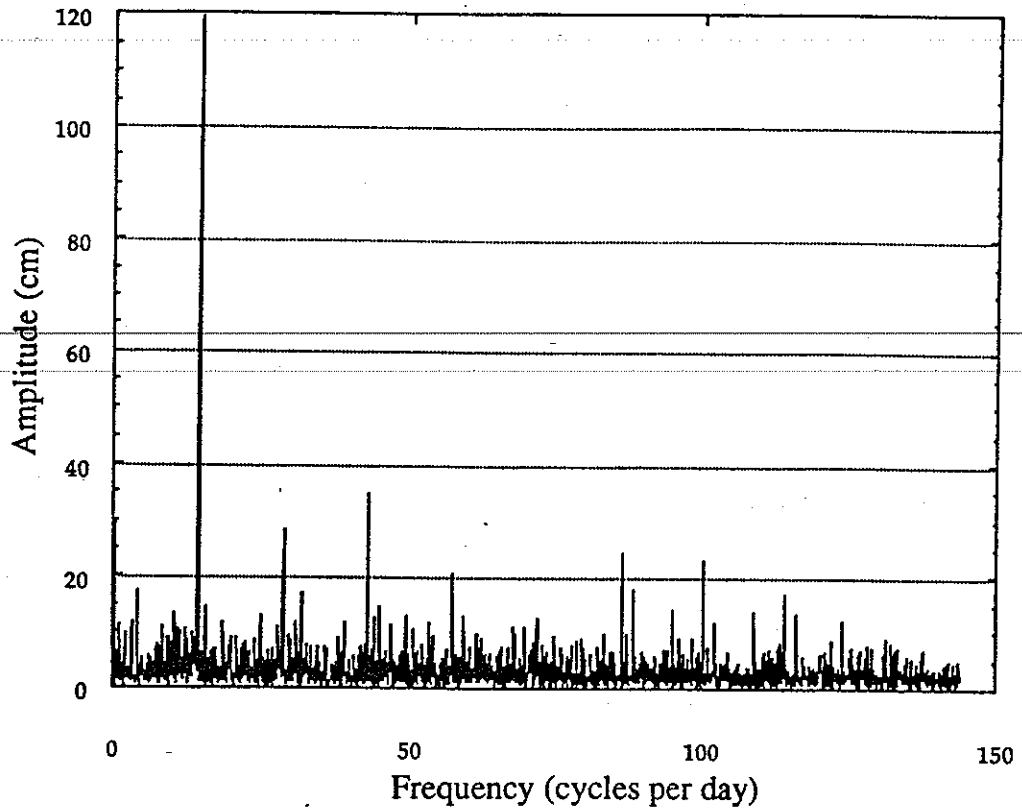

Figure 8 : Periodogram of the Mean Altimeter Data of the cycle 6.

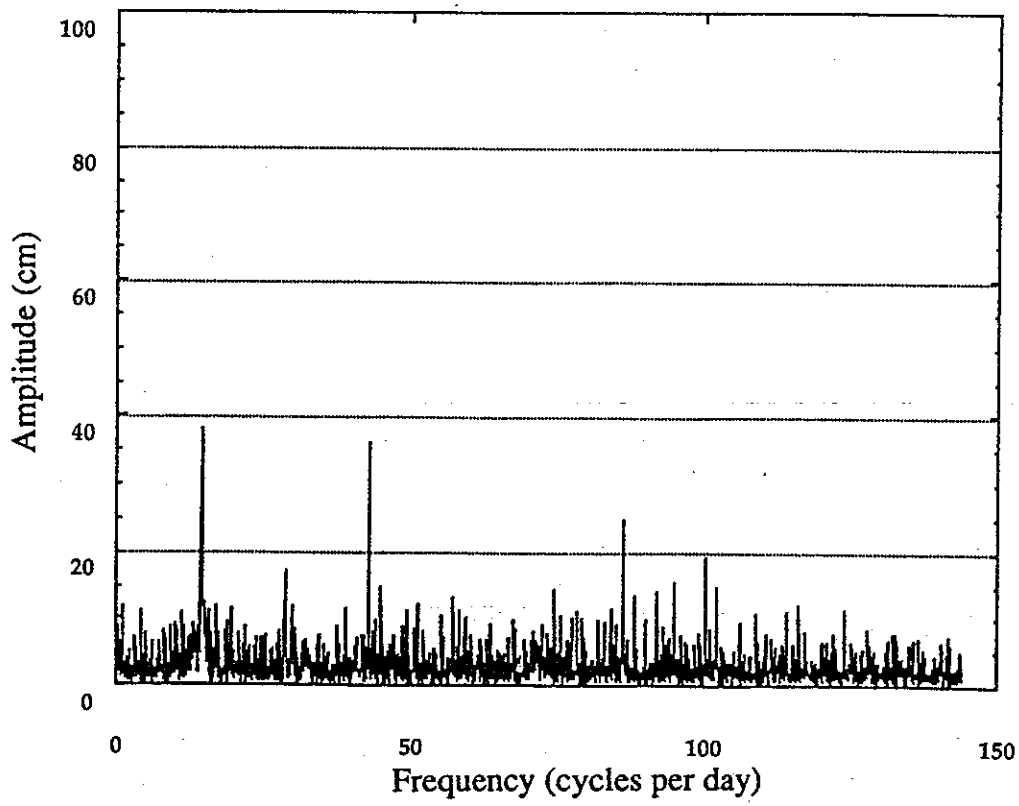

Figure 9 : Periodogram of the Mean Altimeter Data of the cycle 8.

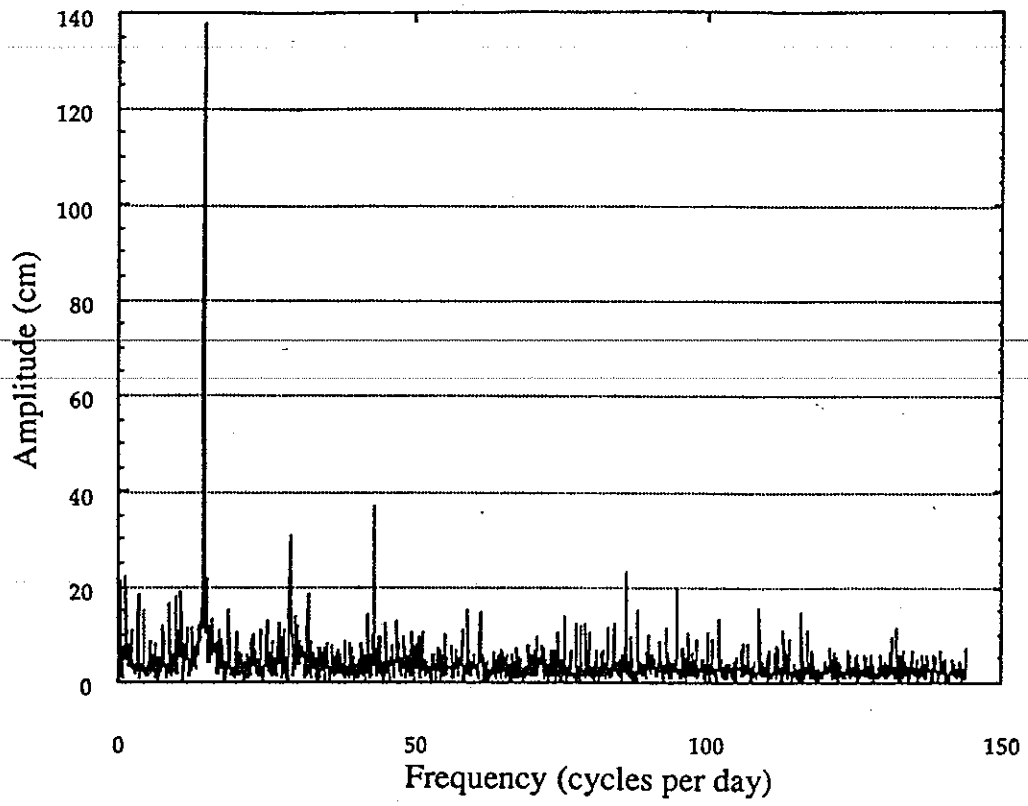

Figure 10 : Periodogram of the Mean Altimeter Data of the cycle 19.

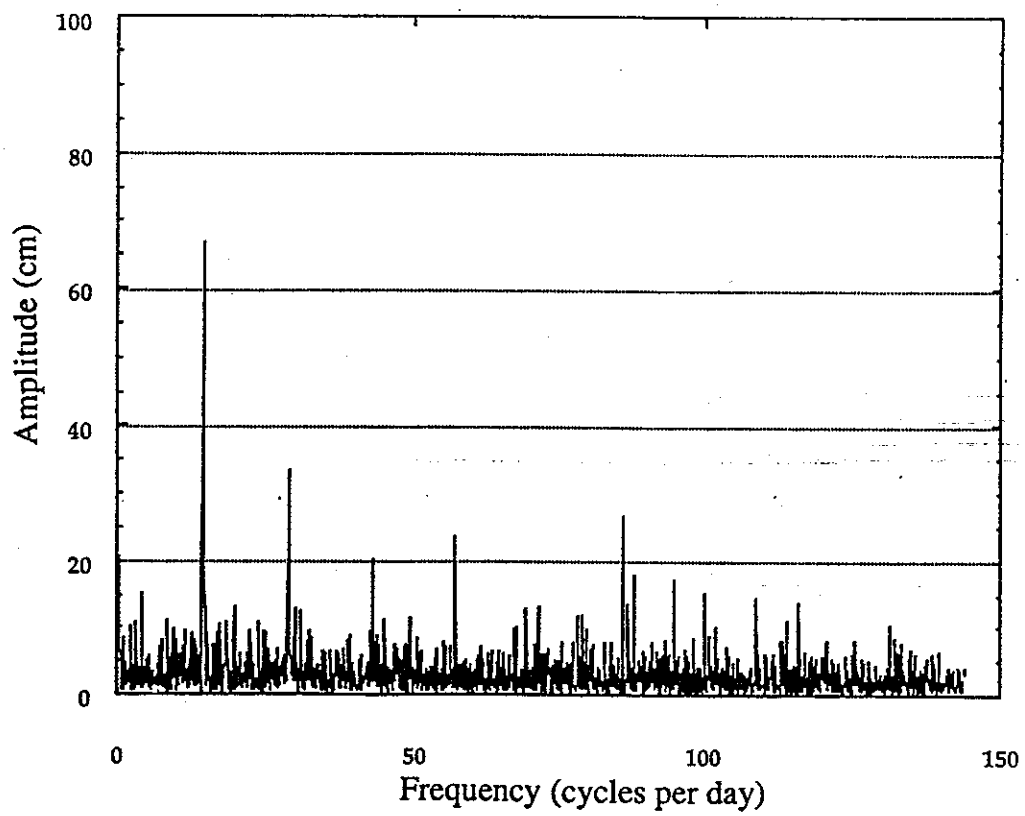

Figure 11 : Periodogram of the Mean Altimeter Data of the cycle 22.

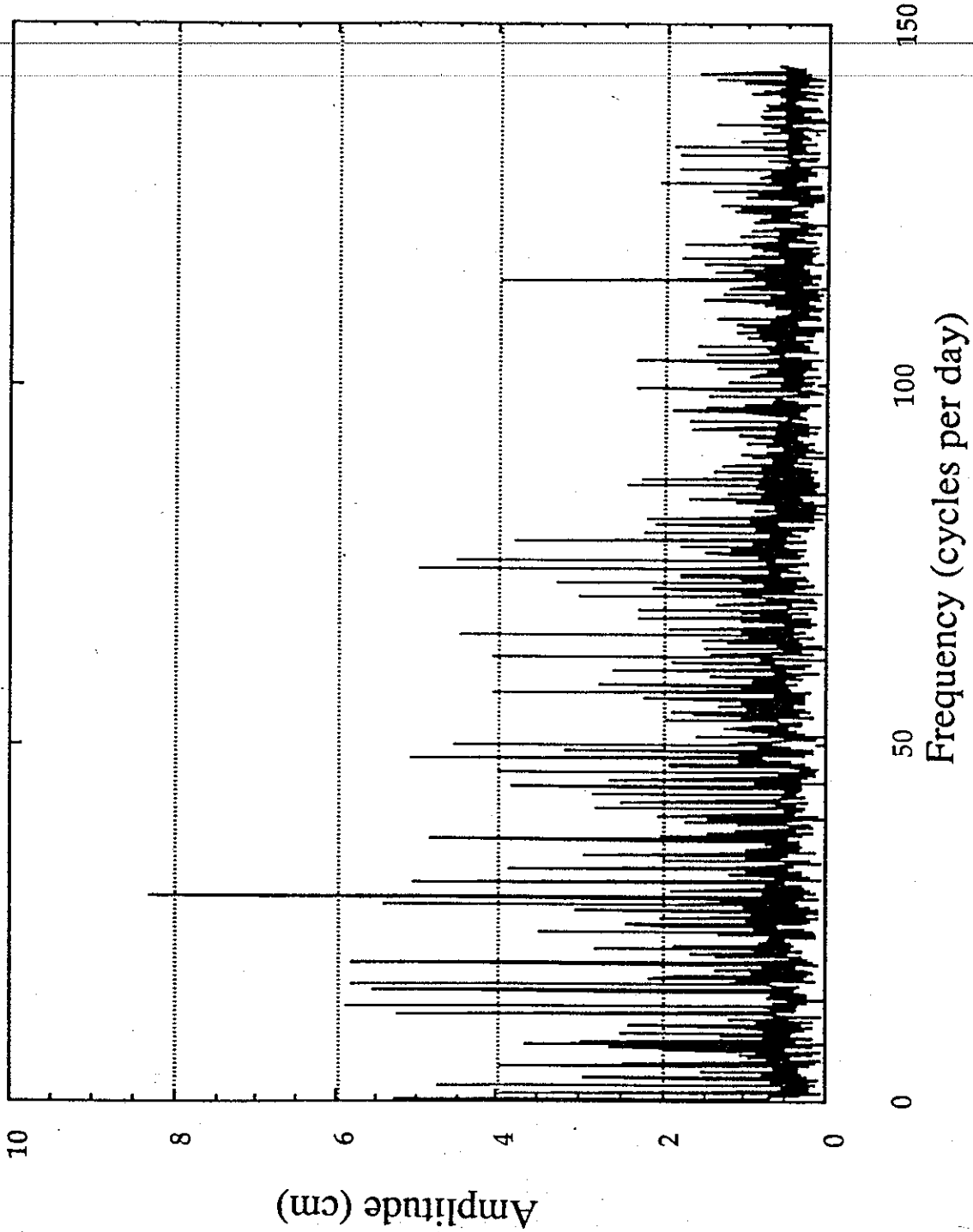

Figure 12 : Periodogram of the tidal height as sampled over the cycle 1.

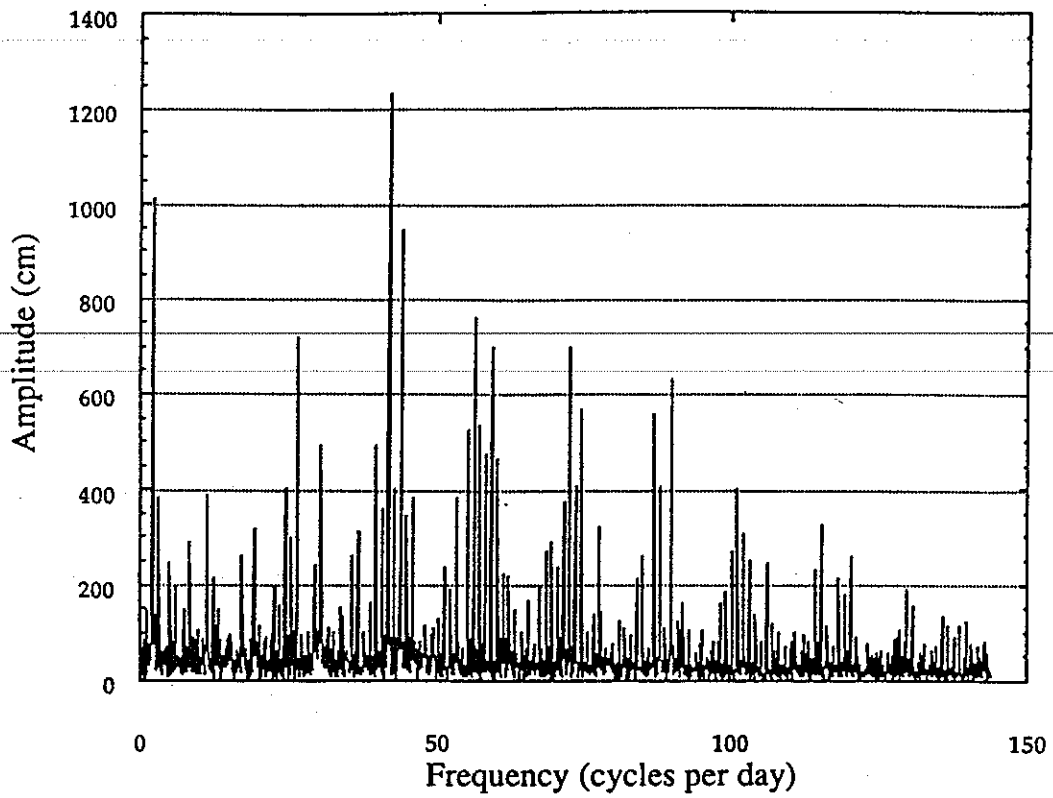

Figure 13: Periodogram of the heights of the geoid as sampled over the cycle 1.

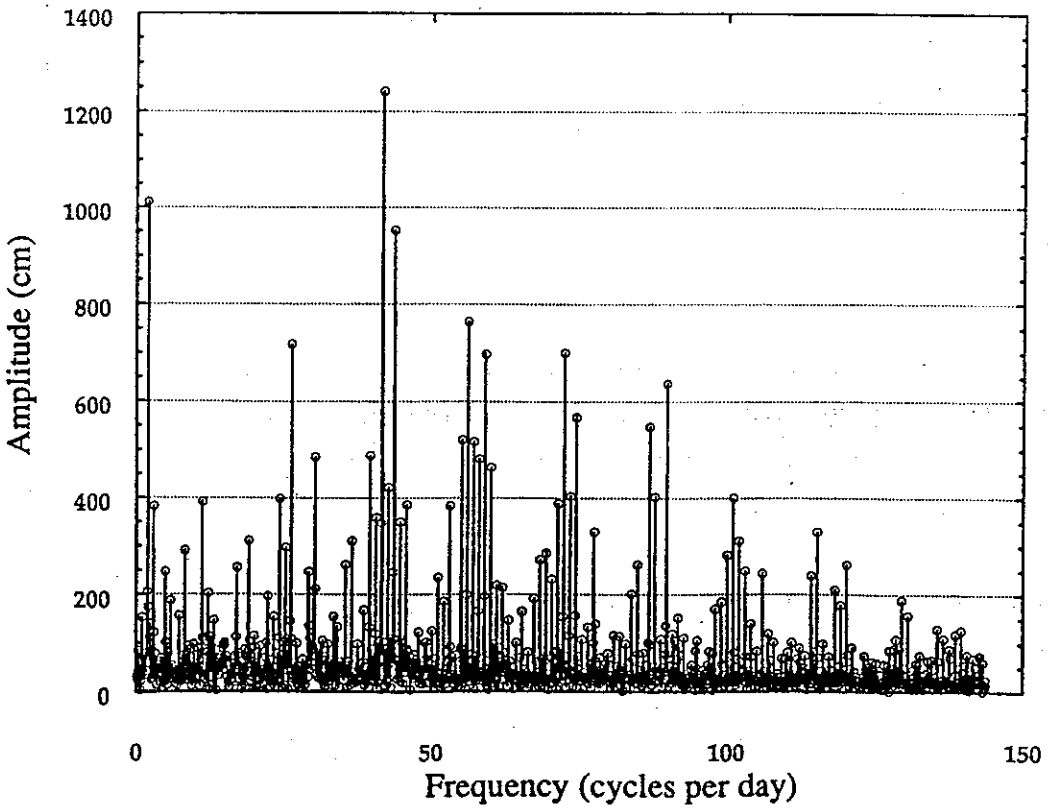

Figure 14: Periodogram of the heights of the geoid plus the Mean Altimeter Data as sampled over the cycle 1.

we want to extract. On the other hand, the comparison of the periodograms of the height of the geoid and of the height of the geoid plus the MAD reveals the predominance of the geoid and the non-negligible role that the errors on the geoid may play.

4.2 Discussion

All the periodograms presented above suffer from the same cumbersome defect. They have been computed on unevenly sampled time series. So, the periodogram of such series is smeared : what is obtained is the periodogram resulting of a convolution of the true spectrum with a spectrum depending on the sampling. In order to illustrate this point, the periodogram of a purely sinusoidal function sampled at the times of the data of the cycle 1 is displayed in Figure 15. There is a weak attenuation of the amplitude but energetic peaks appear at other frequencies. From the knowledge of the time sampling, one can predict the smearing function and theoretically clean the periodogram by a deconvolution. Deconvolution of spectra of Geosat altimeter data has already been tried but with limited success. The principal reason is that the deconvolution is an ill-posed problem. Its resolution requires the use of regularization techniques which are computationally expensive.

There are various reasons to believe that the amplitudes and phases of the detected frequencies by the Fourier Transform of the MAD vary in time. It exists a method called complex demodulation which allows to follow the in-time variations of the amplitude and the phase of a sinusoidal signal. This technique will be applied for the first time to the altimeter data and should eliminated the deconvolution problem.

4.3 Conclusion

The pre-processing of the altimeter data is completed. They have been prepared in an appropriate form for a global inversion of the long wave length phenomena like errors of the geoid and radial orbit error. Preliminary spectral characteristics of the content of the altimeter data have been obtained. There is evidence of the presence of a signal at 1 cycle per revolution and overtones at 2, 3, 4, .., cycles per revolutions probably partially due to the smearing function generated by the unevenly distribution of the data. In addition, the amplitudes of the spectra are not stationary from one cycle to the other and inside the cycle themselves.

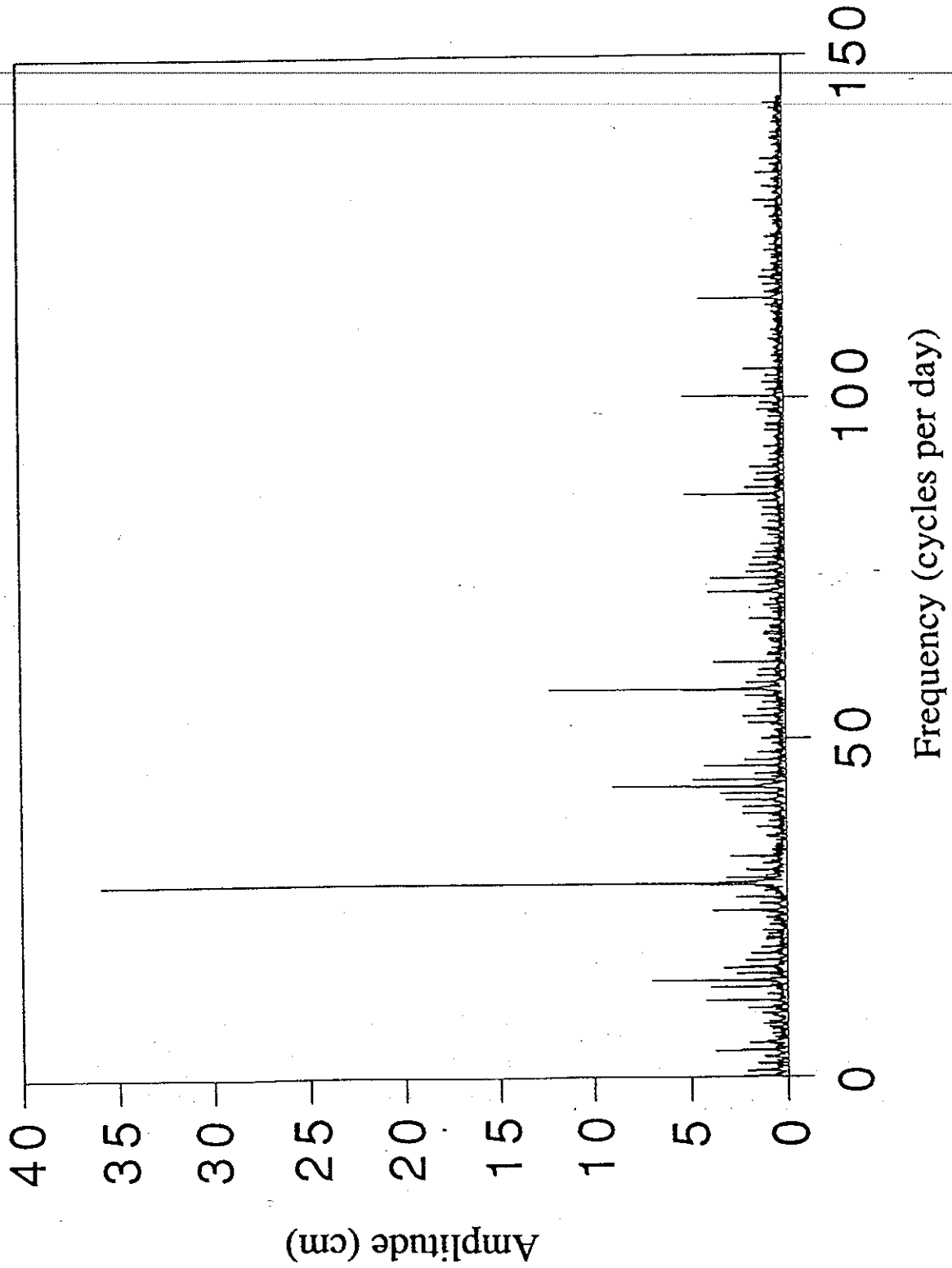

Figure 15: Periodogram of a purely sinusoidal function sampled at the times of the Mean Altimeter Data of the cycle 1. The amplitude is 40 cm at the frequency 28 cycles per day.

5. Complex demodulation

Our present priority consists in improving the radial orbit error models. Indeed, it has been largely shown by different authors (see for example Jourdin et al., 1991) that the accuracy of the ocean tides models deduced from altimetry is mainly limited by the error on the radial position of the satellite. Several approaches for modelling the orbit error have been tried (e.g. Houry et al., 1992) with more or less success.

Periodograms of altimeter data always contain the same trio of largest peaks at 1, 2, 3 cycles per revolution (cy/rev). These harmonics are accredited to the radial orbit error. Fluctuations of their amplitudes and phases have been observed many times. Hence, the harmonic analysis adapted to purely periodic phenomena having simple representation in terms of cosine functions is not adequate to analyze altimeter data. This had motivated the use of the complex demodulation technique which gives the variations of the amplitude and phase as a function of time for a fixed frequency.

A test on a simulated series is given in order to appreciate the performance and the limits of the processing. The results of complex demodulation of real altimeter data for the largest spectral peak are presented. They explain why more sophisticated models of radial orbit error are needed.

5.1 Principle of the complex demodulation

Let x(t) a time series that contains a perturbed periodic component plus a noise component including other harmonics and a noise process

$$x(t) = A(t) \cos[\omega t + \phi(t)] + \varepsilon(t) \qquad (5.1)$$

where $\{A(t)\}$ is a slowly changing amplitude and $\{\phi(t)\}$ is a slowly changing phase. The aim of the complex demodulation (Bloomfield, 1976) is to extract approximations to the series $\{A(t)\}$ and $\{\phi(t)\}$. In a way, it is a local version of harmonic analysis : it is a harmonic analysis since one seeks to describe the amplitude and the phase of an oscillation, and it is local since only data in the neighbourhood of t are used to determine the amplitude and phase.

Writing (5.1) in a complex form, one has

$$x(t) = 0.5\, A(t) \{\exp[i(\omega t + \phi(t)] + \exp[-i(\omega t + \phi(t)]\} + \varepsilon(t) \qquad (5.2)$$

if we let

$$y(t) = x(t) \exp(-i\omega t) \qquad (5.3)$$

we find

$$y(t) = 0.5\, A(t) \exp[i\phi(t)] + 0.5 \exp[-i(2\omega t + \phi(t)] + \varepsilon(t) \exp(-i\omega t) \qquad (5.4)$$

The first term is the one we want. The basic problem in complex demodulation is thus to separate in equation (5.4) the first term from the others. This is possible under some assumptions:

1. $\{A(t)\}$ and $\{\phi(t)\}$ are smooth, then the first term is also smooth.
2. As all the frequencies present in the third term are shifted by $-\omega$ by the complex demodulation, $\{\varepsilon(t)\}$ is assumed to have no component at frequency ω. In any case, any such component cannot be distinguished from $A(t) \cos(\omega t + \phi(t)$. So, $\varepsilon(t) \exp(-i\omega t)$ does not contain component around zero frequency and hence is not smooth.

Finally, the problem consists in extracting the smooth part of y(t). This is easily accomplished by a low-pass filter.

5.2 Special case : the altimeter data

Complex demodulation of altimeter data is complicated by the fact that the altimeter data are unevenly sampled time series. The common linear filtering methods cannot be applied because they are dedicated to evenly time series. In order to overcome this problem, we have developed the following strategy which can be divided into three distinct steps :

1. computation of the Fourier spectrum of the original unevenly spaced series using the Laudet's program (Laudet, 1988).
2. First filtering of the altimeter series and interpolation on equally spaced time values. This second step is realized by using a sophisticated "objective analysis" procedure making use of covariance functions. The chosen covariance functions are pure cosine whose frequencies are the demodulated frequency and the main frequencies of the spectrum computed in the first step. After this second step, the output series is evenly sampled and contains only one cosine component and its modulation.
3. Complex demodulation and filtering by a classical least-squares filter as described in Bloomfield (1976).

The second step is the more crucial. It allows an evenly re-sampling of the series and it eliminates a great part of the noise. This processing is workable if and only if the amount of frequencies present in the Fourier spectrum is no too large. This is

fortunately the case for the altimeter data series as the spectrum of 51 days of Geosat altimeter data with Gem-T1 orbit (Figure 19) testifies.

5.3 Complex demodulation of a simulated series

The procedure described in the previous section has been applied on a series whose modulation of the amplitude and phase at a given frequency is known. For this test, cycle 1 of the Geosat altimeter data pre-processed as indicated in chapter 4 has been used. The harmonic analysis reveals a dominant energetic peak at 14.254 cycles per day which corresponds to 1 cycle per revolution. All the other energetic peaks appear at overtones 2, 3, 4, ... cycles per revolution. A new series has been constructed simply by adding a modulated cosine function at the altimeter data series of cycle 1. The frequency of the cosine is 21 cycles per day corresponding to a spectral band of weak energy. Hence, our strategy of complex demodulation can be tested under realistic conditions and the performance can be estimated as the sought signal is known. Figure 16 shows the periodogram of the simulated series. The 1 cycle per revolution and overtones peaks clearly appear. The arrow indicates the added modulated cosine function. The spectrum which is used to form the covariance functions of the objective analysis is displayed in Figure 17.

In Figures 18, the real modulation (dashed line) is compared with the result of the complex demodulation (full line). The complex demodulation is very efficient in recovering the linear part of the modulation. The less successful but nevertheless acceptable result for the non-linear part is due to the transfer function of the objective analysis which tends to smooth too much the signal.

5.4 Complex demodulation of Geosat altimeter data

Geosat altimeter data of cycles 1, 2 and 3 have been put all together. It is represents an unevenly sampled time series of about 37,000 data covering 51 days. The periodogram of this series and its spectrum (Figures 19 and 20) contain three largest peaks at 1, 2 and 3 cycles per revolution, respectively. In chapter 4, we emphasized the variability of the amplitude and phase of the peaks from one cycle to the other. The complex demodulation of these three frequencies should clearly prove these fluctuations not only from one cycle to the other but also inside the cycles themselves.

Firstly, the series has been demodulated at the 1 cy/rev frequency. The time series of the fluctuations of the amplitude and phase at this frequency are displayed in Figures 21. The most important feature is the large variation of the amplitude between

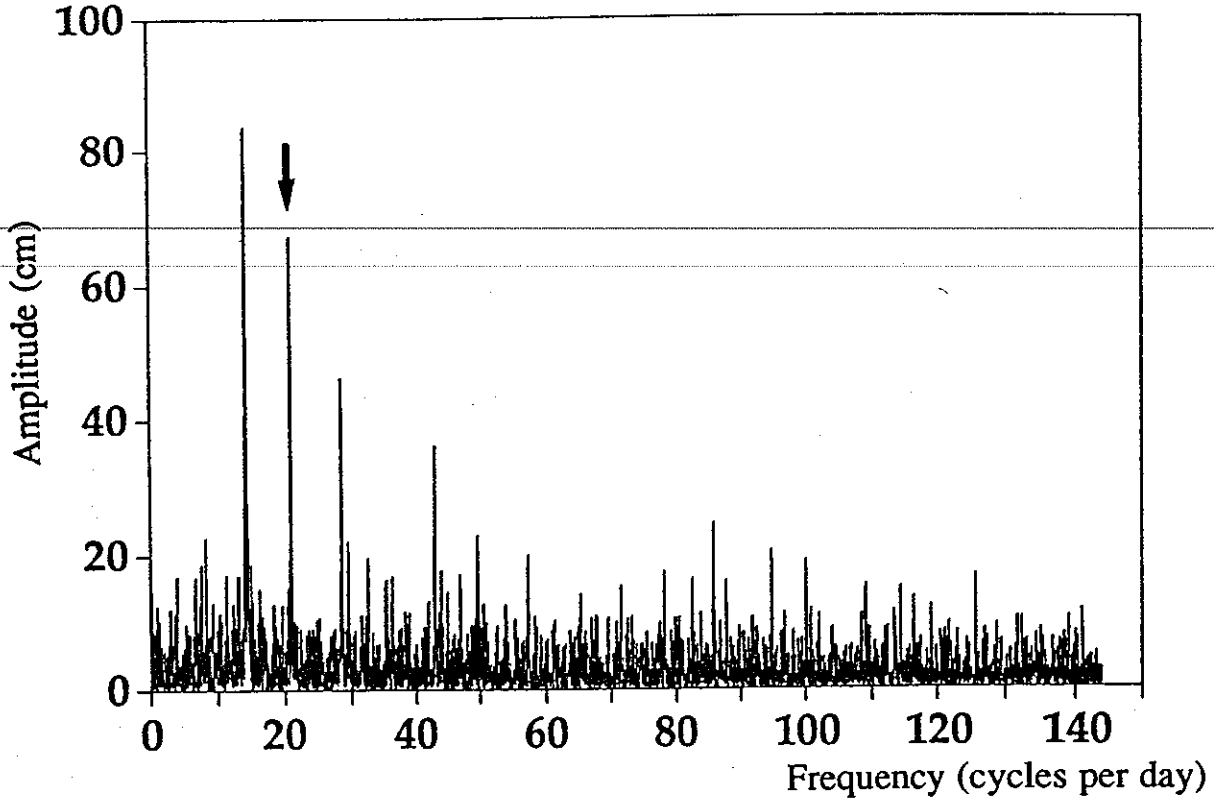

Figure 16: Periodogram of the Geosat altimeter data of cycle 1 plus a modulated cosine function at 21 cycles per day (arrow).

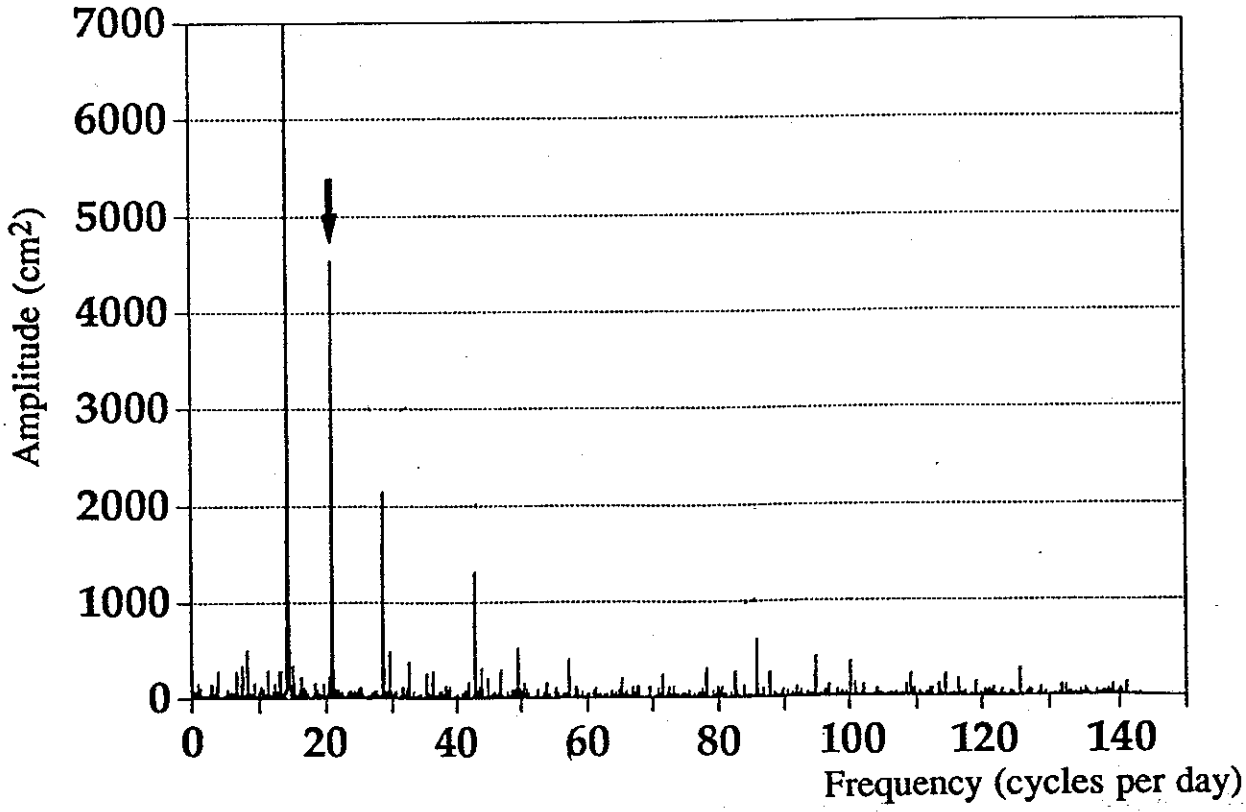

Figure 17: Spectrum of the Geosat altimeter data of cycle 1 plus a modulated cosine function at 21 cycles per day (arrow).

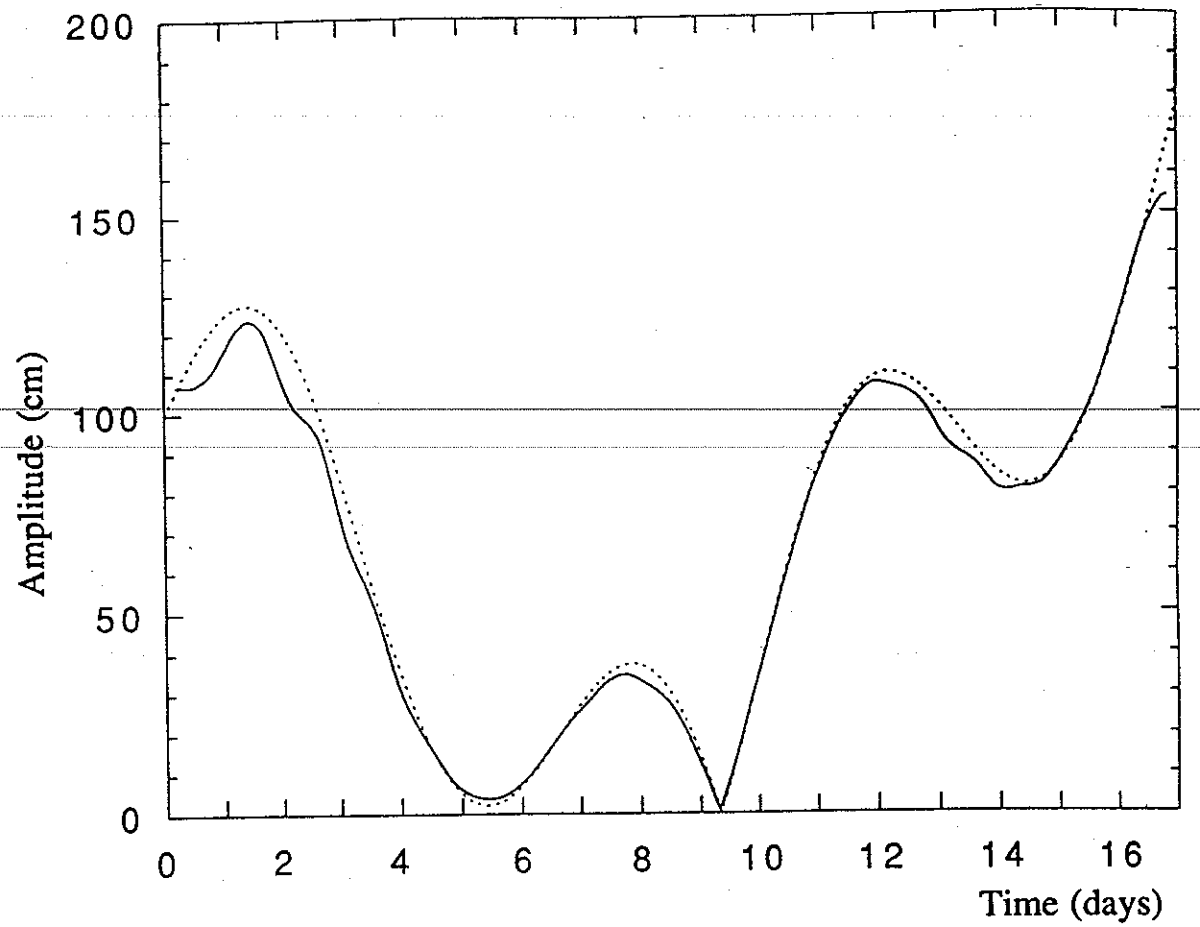

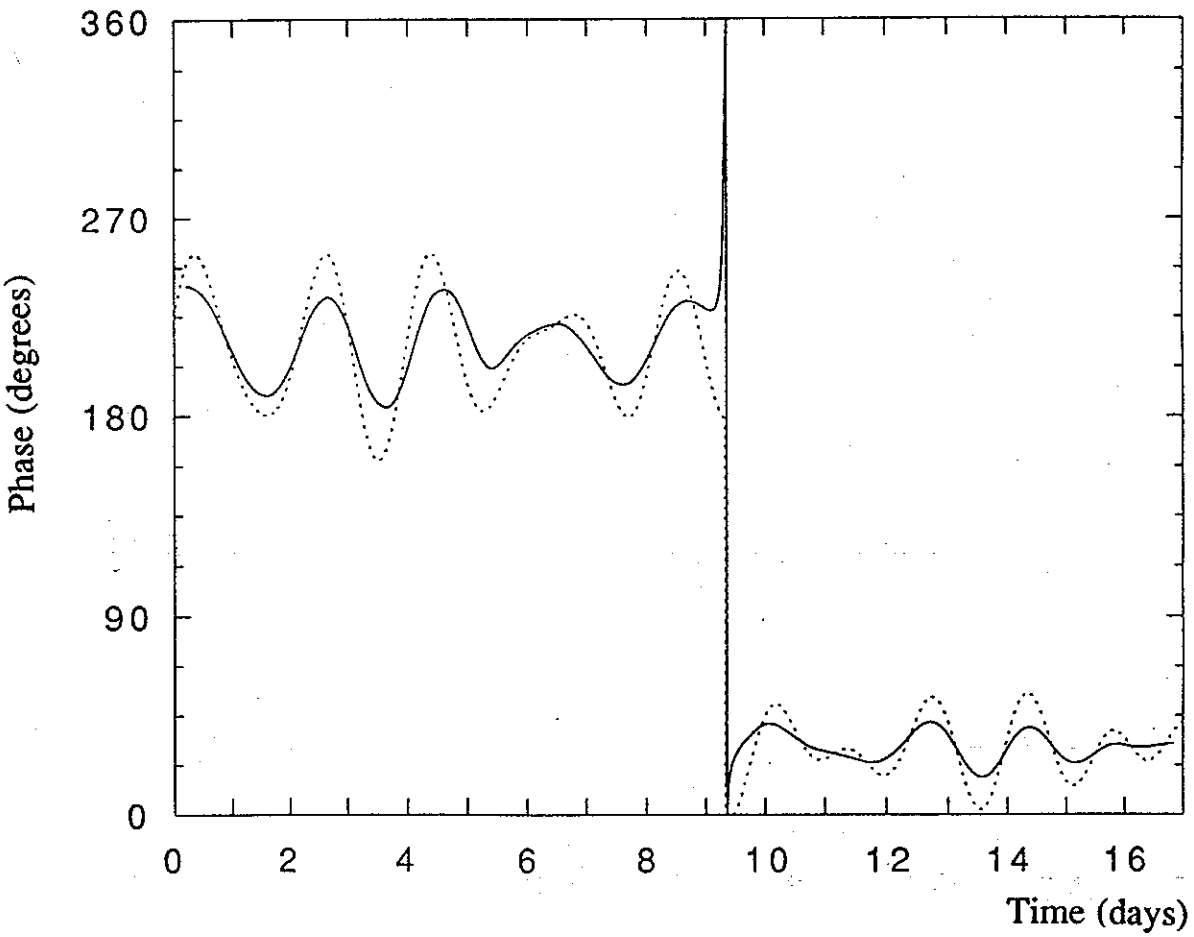

Figures 18: Amplitude and phase of the complex demodulation (full line) and of the modulation (dashed line) of the simulated serie at the frequency of 21 cycles per day.

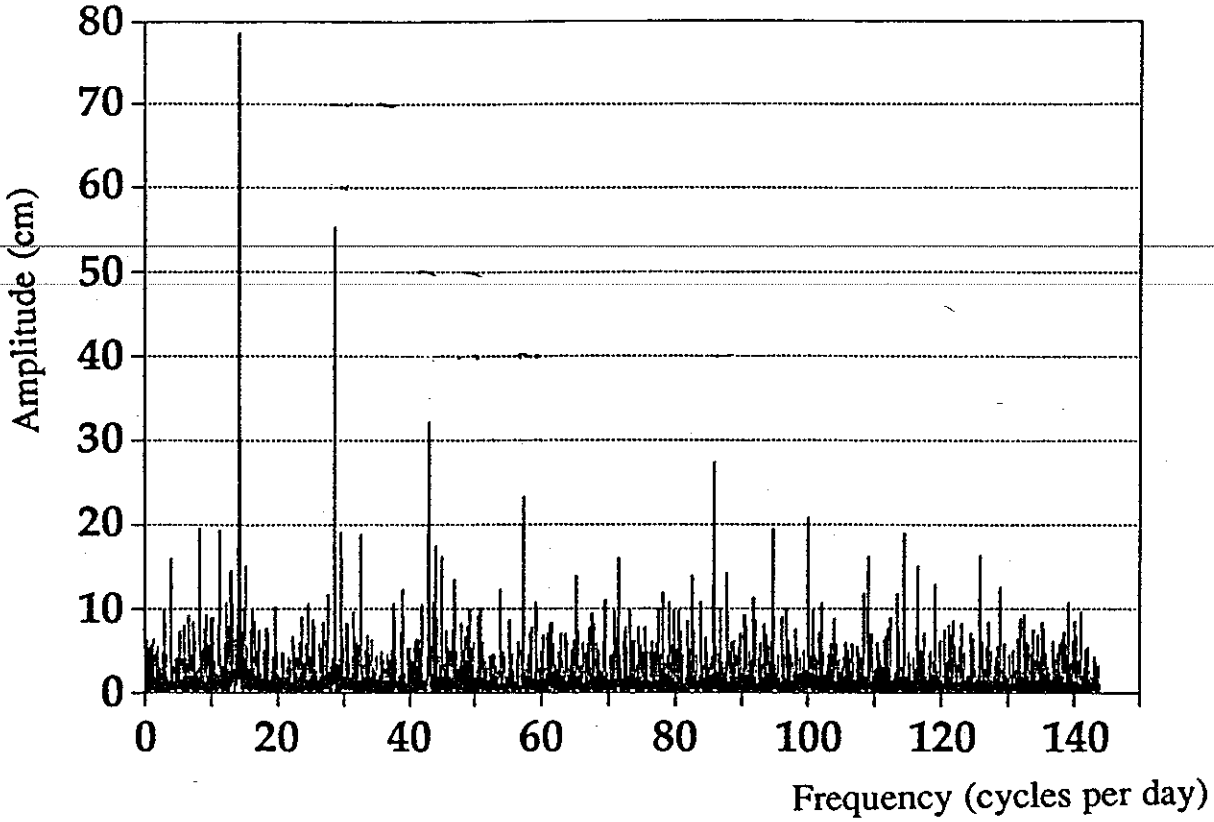

Figure 19: Periodogram of the Geosat altimeter data of 51 days equivalent to 3 cycles.

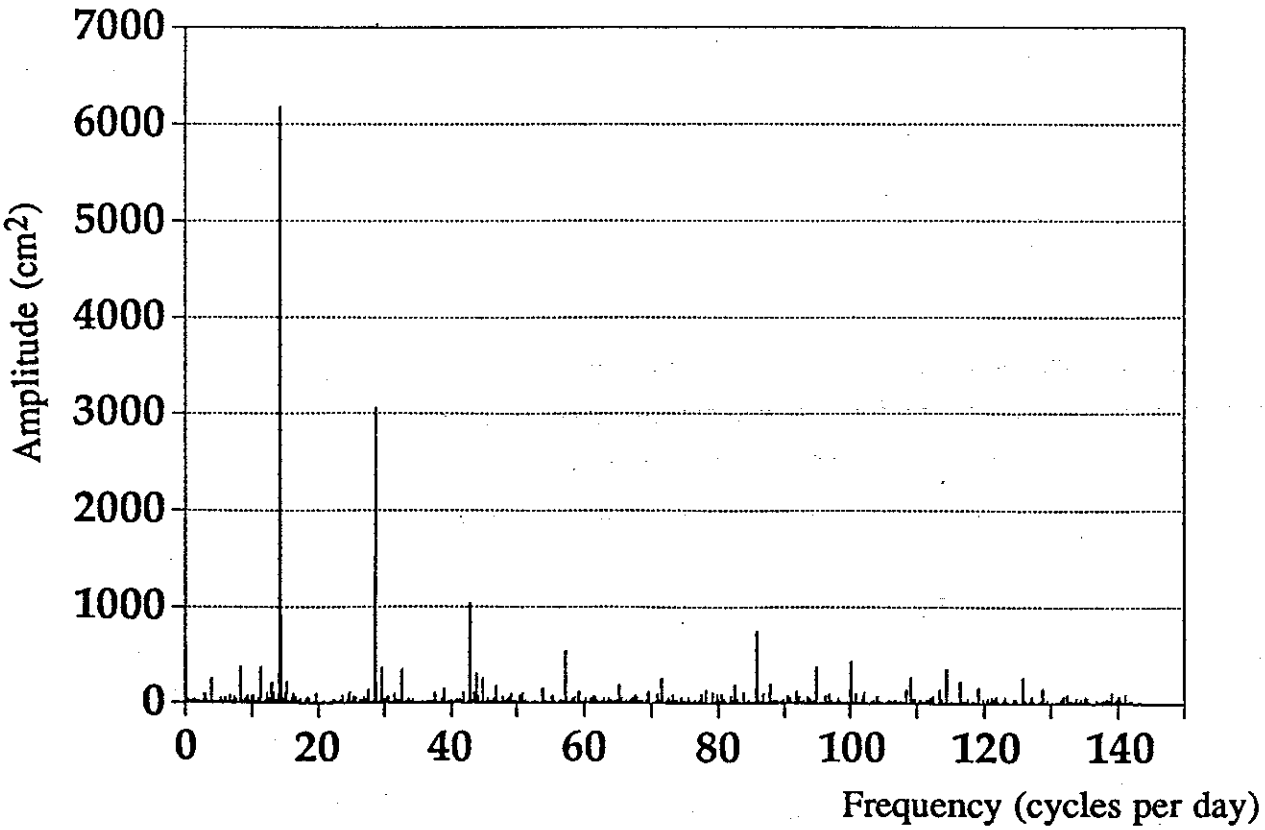

Figure 20: Spectrum of the Geosat altimeter data of 51 days equivalent to 3 cycles.

20 cm to 190 cm, whereas the phases vary from 70 degree to 210 degree. Yet, there is not significant periodic character in the modulation of the 1 cy/rev harmonic. In order to verify these results, the amplitudes and the phases of the 1 cy/rev frequency have been computed on sub-series covering 3 days for a 17 days period equivalent to one cycle. The dots of the Figure 22 are the successive values as obtained by this "moving" harmonic analysis. They are located at the middle time values of each of the sub-series. There is an excellent agreement for the amplitudes between the two methods while there is a slight shift of the phases. On the other hand, the modulated 1 cy/rev oscillation has been computed at the time values of the original series by using the time series of the fluctuations of the amplitude and phase (Figure 21). Then, this component was subtracted from the original series. The periodogram of the series of residual is given in Figures 23 where it is compared with the periodogram of the original series. The experience shows the efficiency of the method in removing a spectral peak and its associated modulation.

Complex demodulation of the 2 cy/rev (Figures 24) shows large erratic variations of the amplitude while the phase is more stable. At first sight, the complex demodulation of the 3 cy/rev (Figures 25) seems more interesting. Indeed, there is a periodicity of 17 days of the modulation of the amplitude corresponding exactly to the duration of the cycle. These are the very preliminary results of the application of the complex demodulation to altimeter data. It gives us a new vision in the spectral domain opening new exciting questions : for example, it is necessary to identify whether the observed modulations results from dynamical factors (e.g. resonance with gravity field errors, or secular effects of drag) or are simply effects of the numerical orbit calculation.

5.5 Conclusion

The complex demodulation method has intensively been applied to Geosat altimeter data to prove once for all the non-stationarity of the radial orbit error. The origins and the mechanism generating the radial orbit errors are discussed in details in Francis and Bergé (1992). Moreover it is shown how the complex demodulation method can be useful to estimate radial orbit errors.

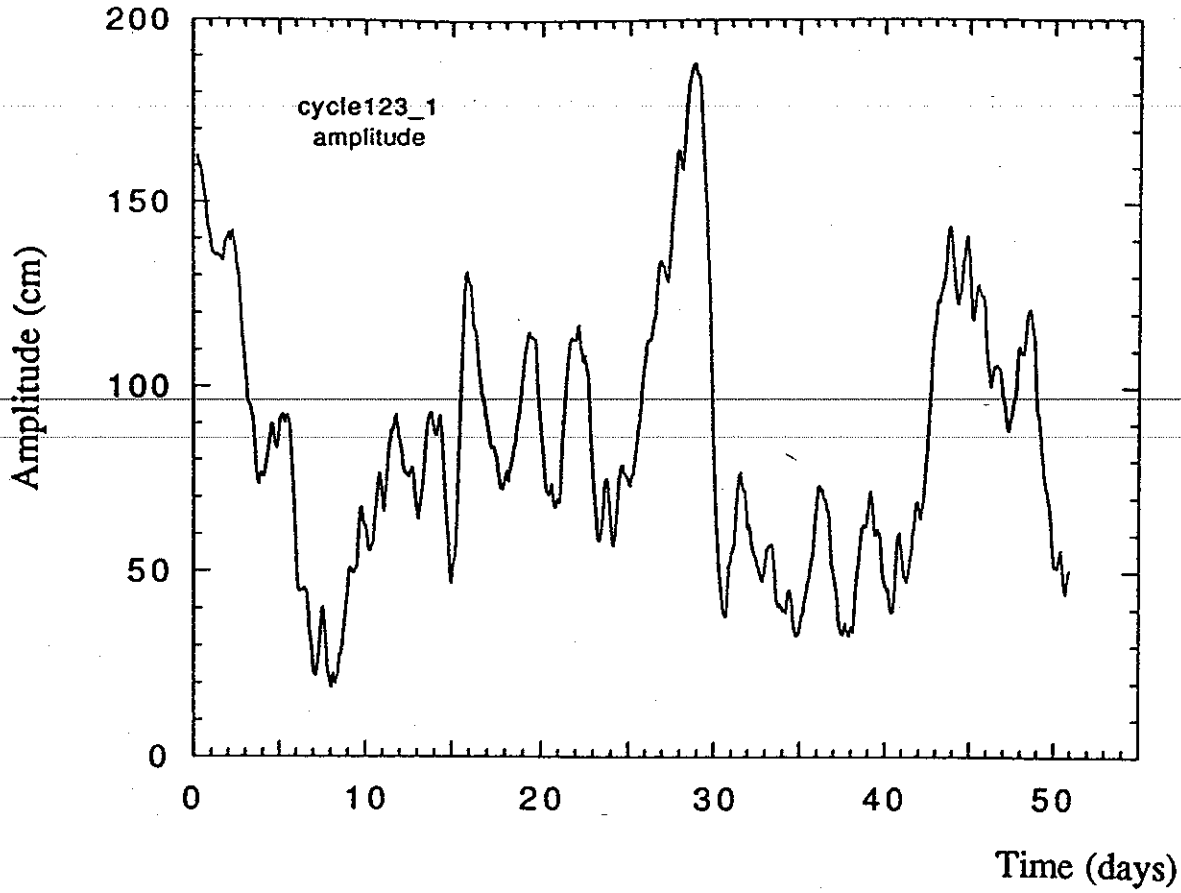

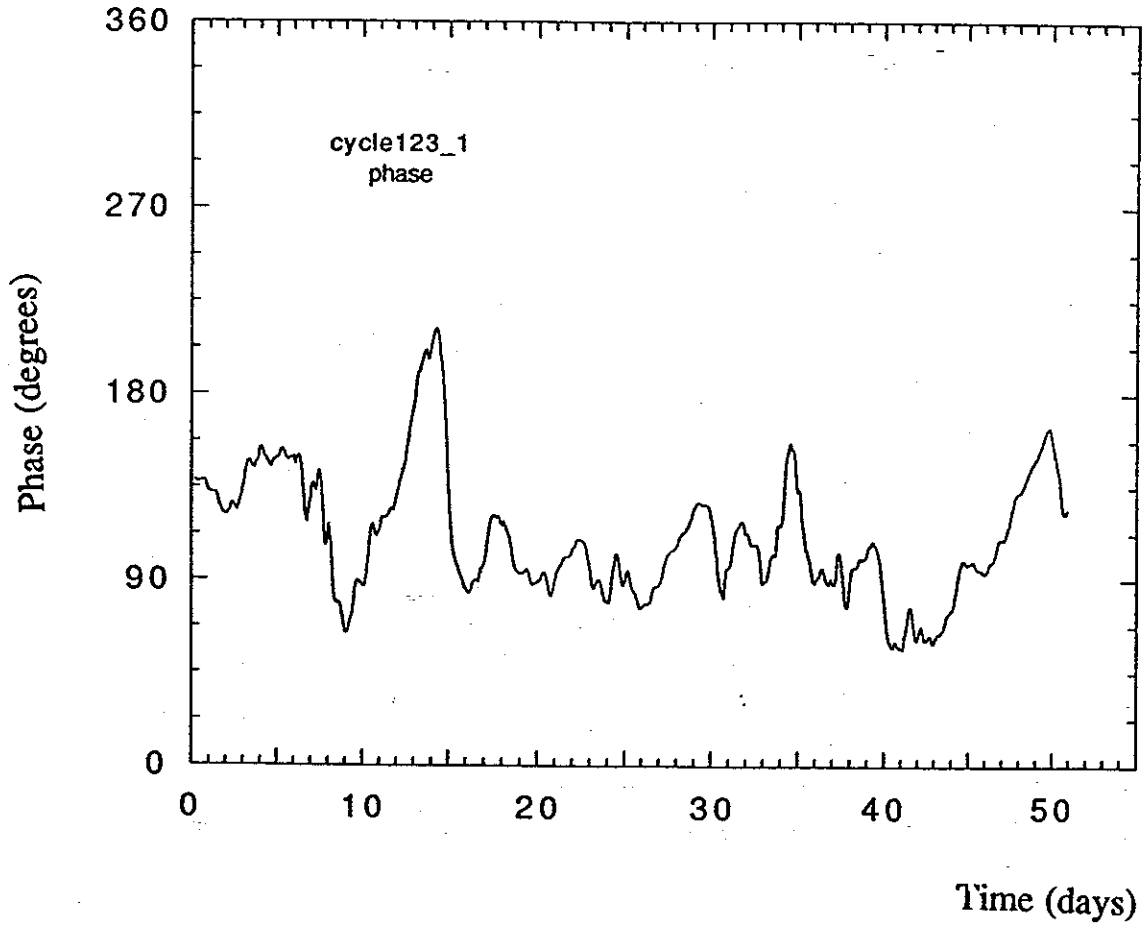

Figures 21: Amplitude and phase of the complex demodulation of 51 days of Geosat altimeter data at the frequency of 1 cy/rev.

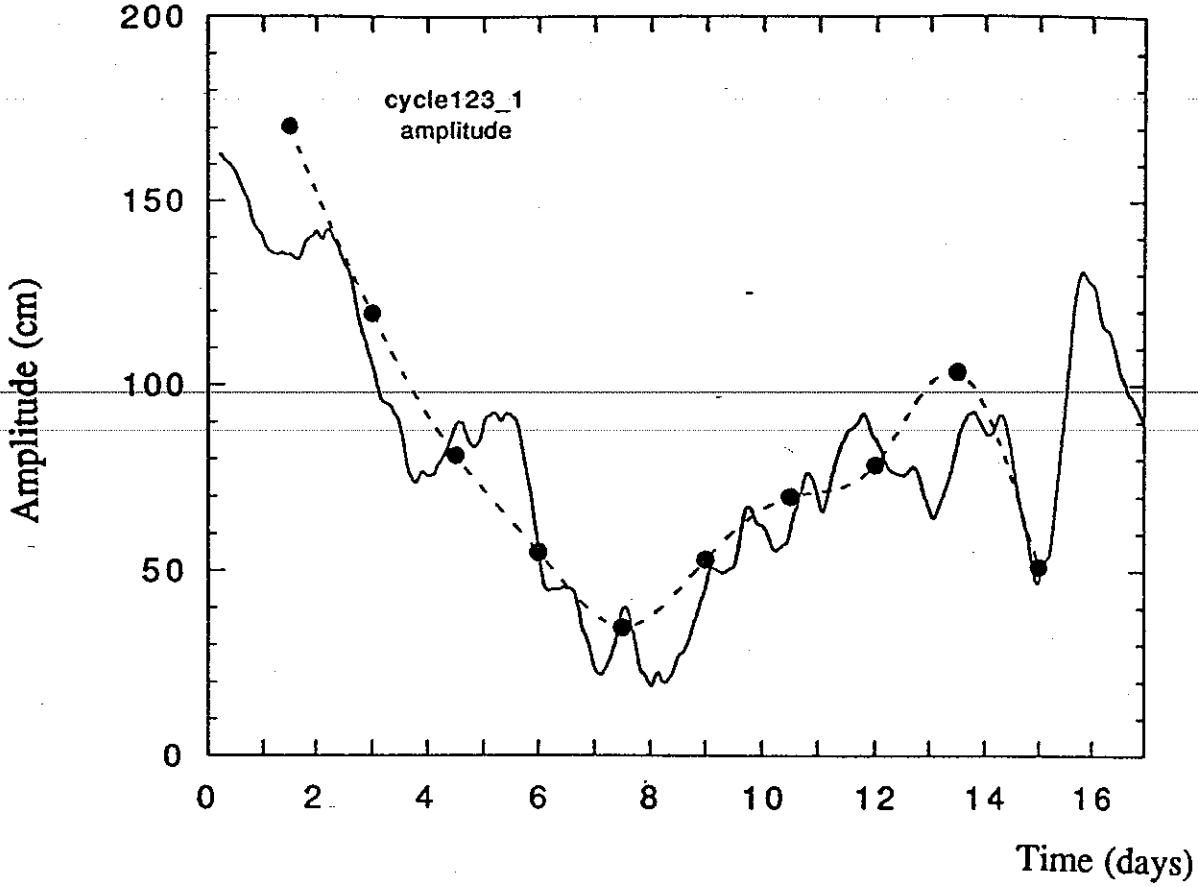

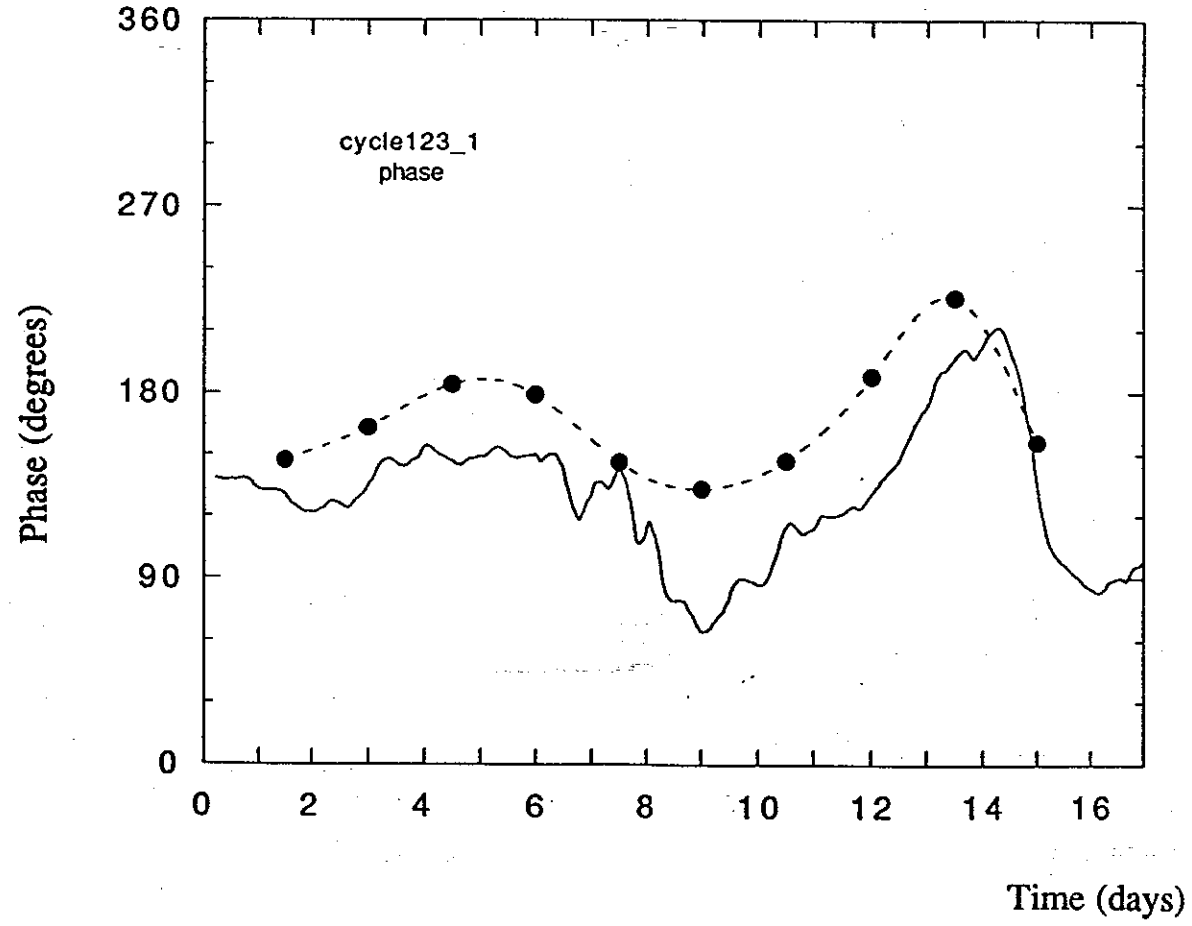

Figures 22: Amplitude and phase of the complex demodulation of 17 days of Geosat altimeter data at the frequency of 1 cy/rev. Dots are the results of harmonic analysis on three days.

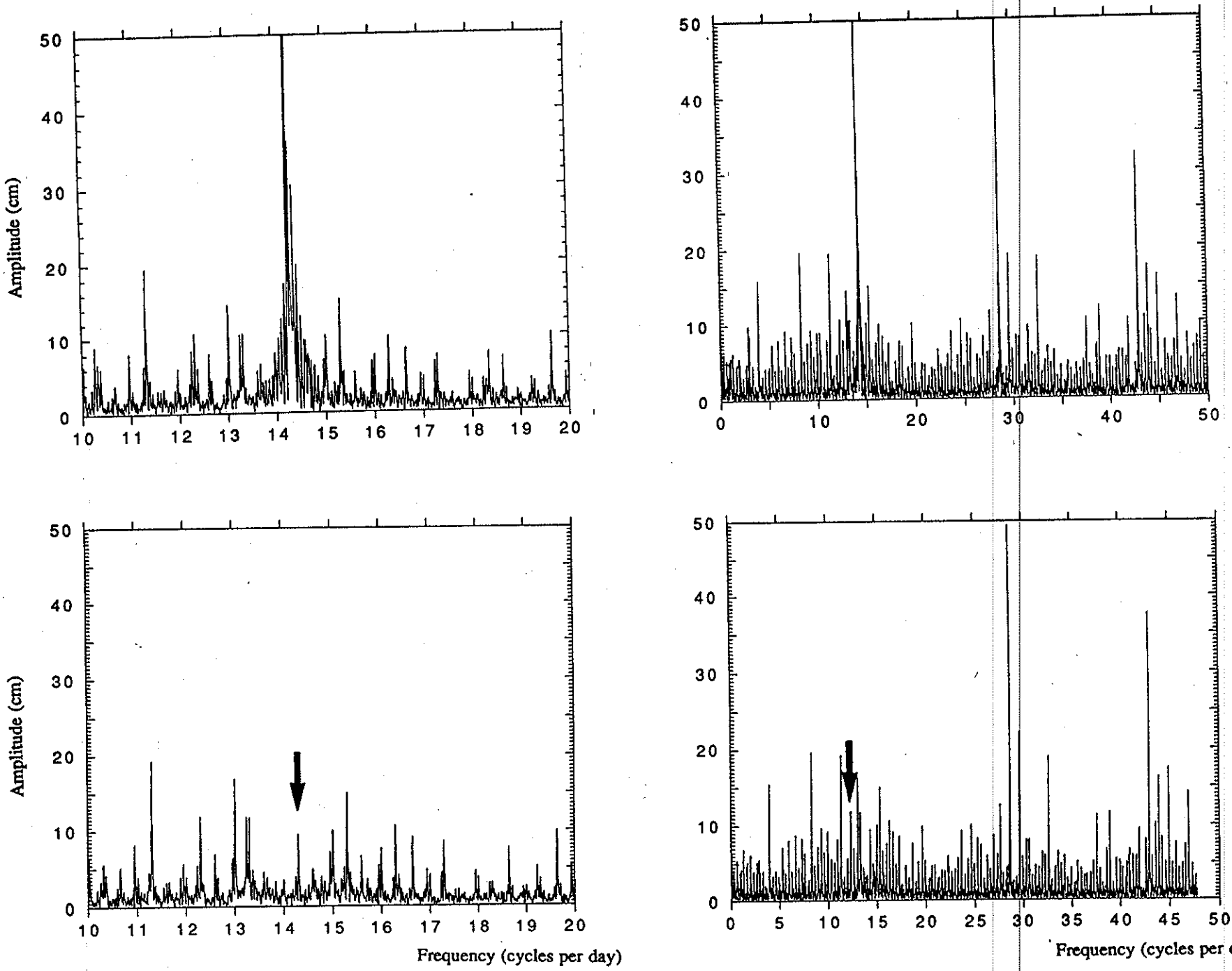

Figures 23:
Periodograms of 51 days of Geosat altimeter data before (above) and after (below) removing the modulated cosine component at 1 cy/rev.

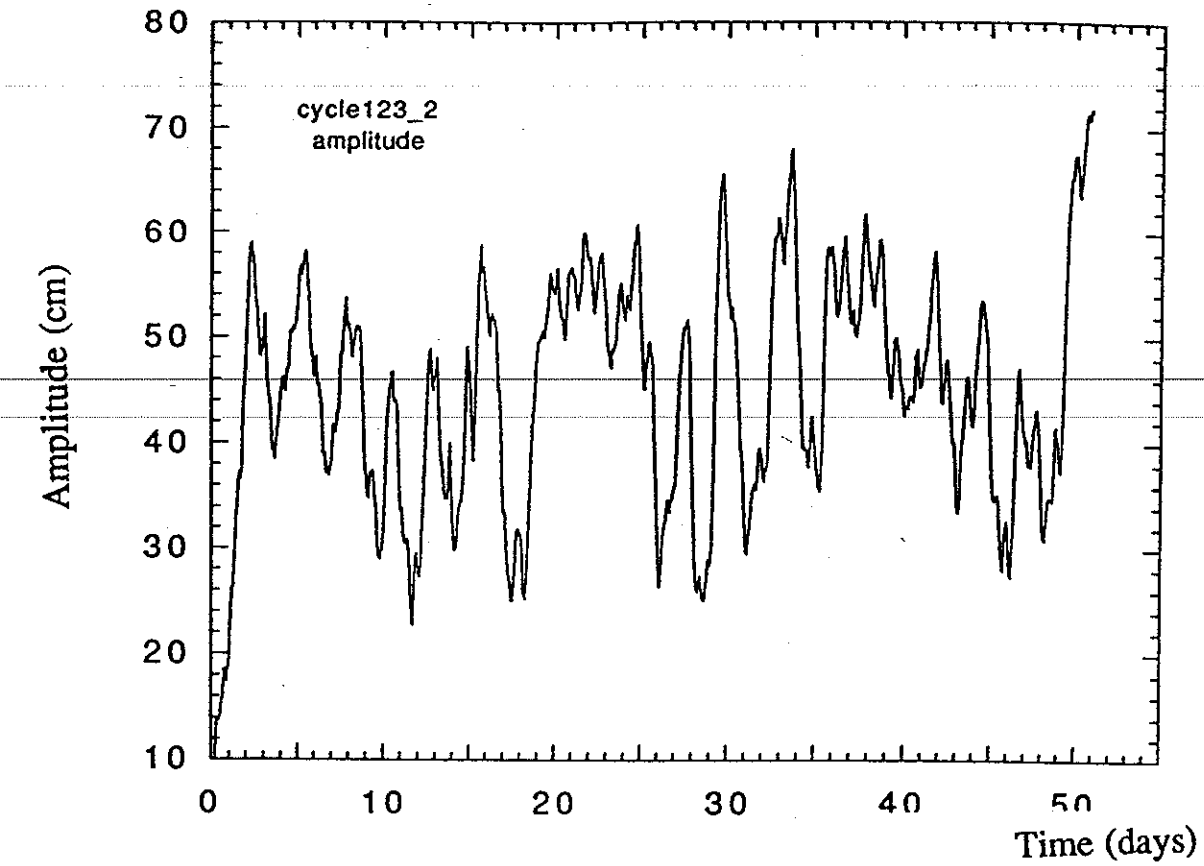

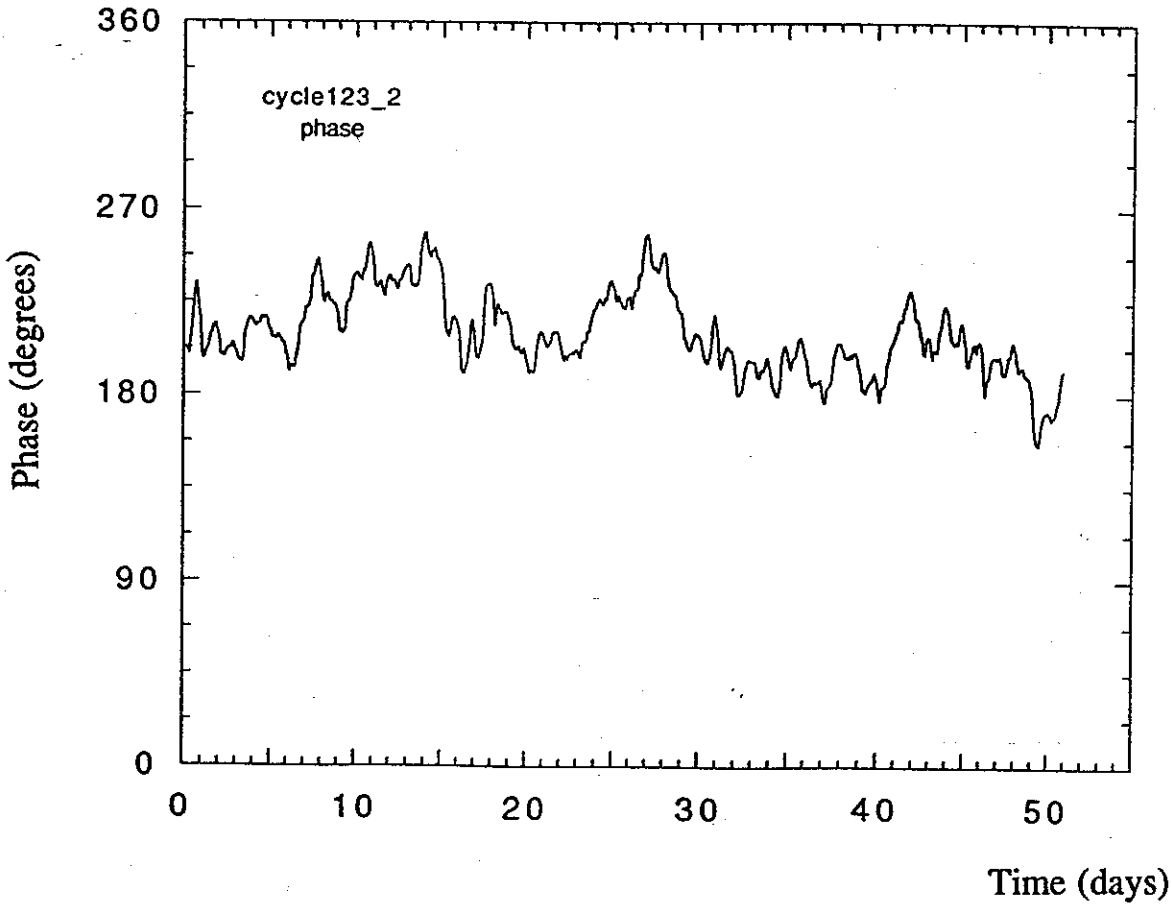

Figures 24: Amplitude and phase of the complex demodulation of 51 days of Geosat altimeter data at the frequency of 2 cy/rev.

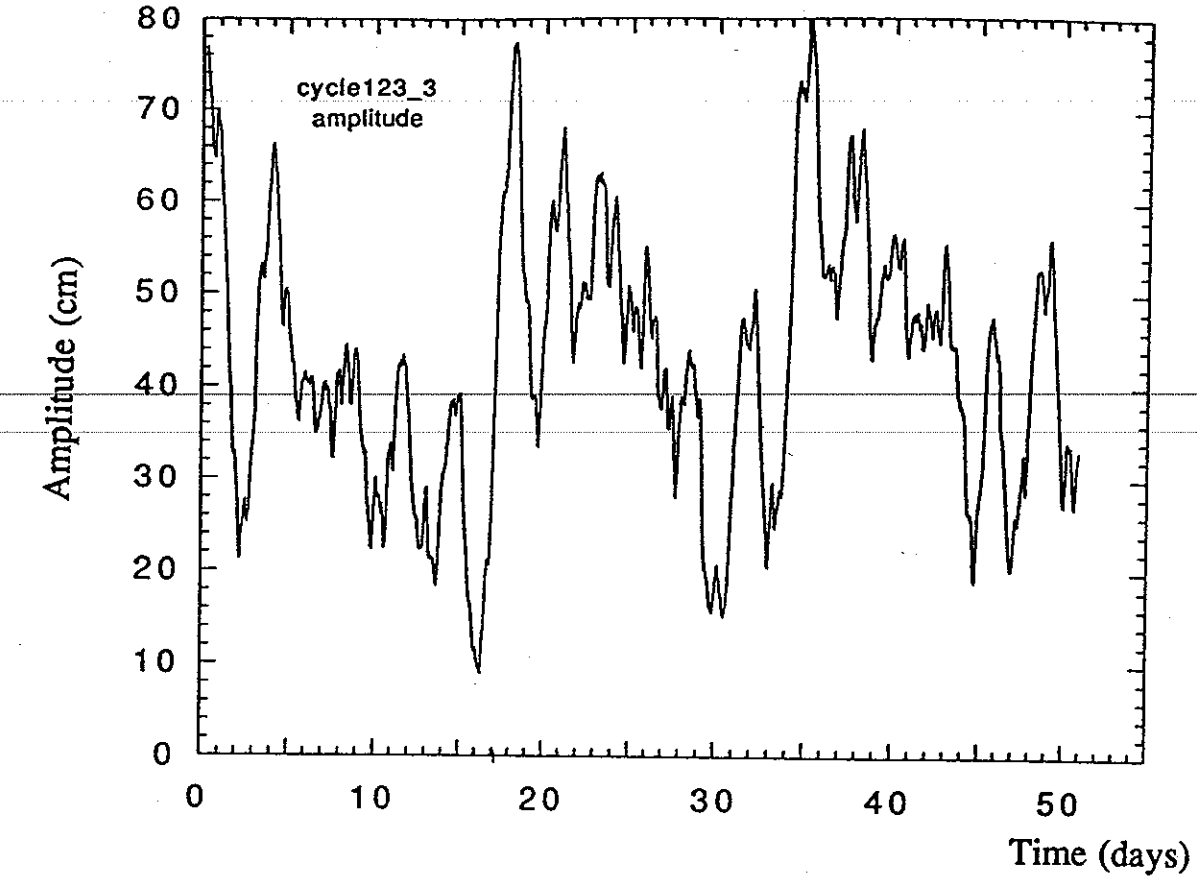

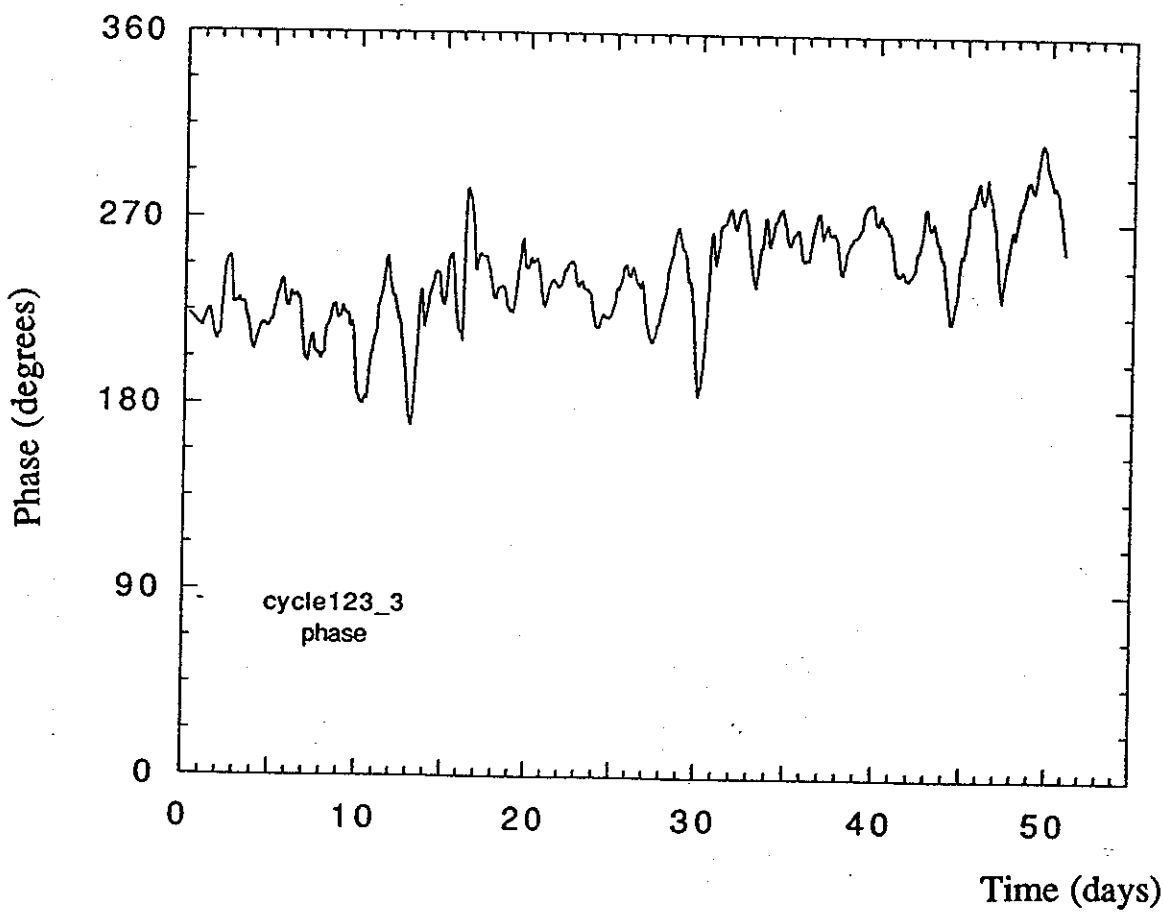

Figures 25: Amplitude and phase of the complex demodulation of 51 days of Geosat altimeter data at the frequency of 3 cy/rev.

6. Oceanic tides from Geosat altimetry

Our objective is to compute global oceanic cotidal maps by inversion of tide gauge, gravity loading and altimeter data. Up to now, global solutions for the ocean tide have been already obtained by using tide gauge and gravity loading data (Francis and Mazzega, 1990a; 1991). The inversion of altimeter data is more difficult because of the huge amount of data and their complex error budget. Among these errors, the major component is certainly the radial orbit errors. Reducing this contribution is an essential step before analysing altimeter data. The application of the complex demodulation method to Geosat altimeter data proved very relevant to estimate the radial orbit error. In the future, this method will be systematically applied to the Geosat altimeter data which will be used in the inversions.

Mazzega and Bergé have developed an algorithm to invert altimeter data as well as to jointly invert altimeter and tide gauge data in order to recover the ocean tides and the mean sea surface over the whole ocean. The computer code has been tested and is now operational. A brief description of the method is given and the first preliminary results are presented. These results, which are very encouraging, permit to test the feasibility of the proposed method in real conditions. In addition, this first experiment provides some indications which will be taken into account to obtain the best possible solutions.

6.1 The inverse method

Our approach consists in mapping ocean tides by objective analysis or inverse method. We use the formalism of the inverse theory described in Tarantola (1987). Succinctly, the following equations are used to predict the expected signal (P) and the covariance of its associated error (C_{pp}) :

$$P = C_{P_0P_0}\, S^{-1}\, d_o$$

$$C_{P\,P} = C_{P_0P_0} - C_{P_0P_0}\, S^{-1}\, C_{P_0P_0}$$

with

$$S = C_{d_0d_0} + C_{P_0P_0}$$

where d_0 = altimeter data vector

C_{d0d0} = a priori covariance matrix describing the altimeter data errors
C_{P0P0} = a priori covariance matrix of the oceanic tide signal
S = square symmetric definite positive matrix sized by the number of data
P = a posteriori estimation vector of the oceanic tide signal
C_{PP} = a posteriori covariance matrix of the error estimation on P

The a priori information ensures the stability of the computation and the unicity of the solution. The a posteriori covariance matrix C_{pp} contains information on the formal accuracy and on the resolution of the estimated signal.

Mazzega and Houry (1989) experimented the inverse method for estimating the mean sea surface from altimeter data in the Mediterranean Sea. More recently, Mazzega and Jourdin (1991) inverted altimeter data to calculate tidal harmonics at several point locations. These pioneer works showed the computational feasibility of the inverse approach as well as its promising potential. Additionally, they furnished the way to obtain the a priori covariance matrices. Nevertheless, two problems remained to be solved : (1) the first experiments showed that the chosen stationary covariance for the radial orbit error is too simple and limits the accuracy of the solution, a better way to remove the orbit error must be investigated. This justified our work presented in section I.2.; (2) up to now only regional or point solutions were computed, as the computation of global solutions requires the processing of a large number of data and the inversion of big systems of equations.

6.2 Preliminary results

Global inverse solutions for the 8 principal constituents of the oceanic tides (M_2, N_2, S_2, K_2, P_1, O_1, K_1, Q_1) have been computed. They result from the average of 22 separate inversions of 12,000 Geosat altimeter data. The resolution of the maps is 1° x 1°. Figures 26 and 27 show the corange and cotidal maps of the major constituent M_2. The results are very encouraging in comparison with Schwiderski's hydrodynamical model (Figures 28) (Schwiderski, 1980a-b). Another example is the Q_1 tidal wave whose amplitude is of the order of 1 centimetre which is relatively well recovered (Figures 29 and 30 to be compared with Figures 31) while the radial orbit error is of the order of 1 meter.

In this first attempt, simplifications have been done : only 264,000 Geosat altimeter data were used; there is no tide gauge data; the various covariances are stationary; the radial orbit error was not estimated by the complex demodulation

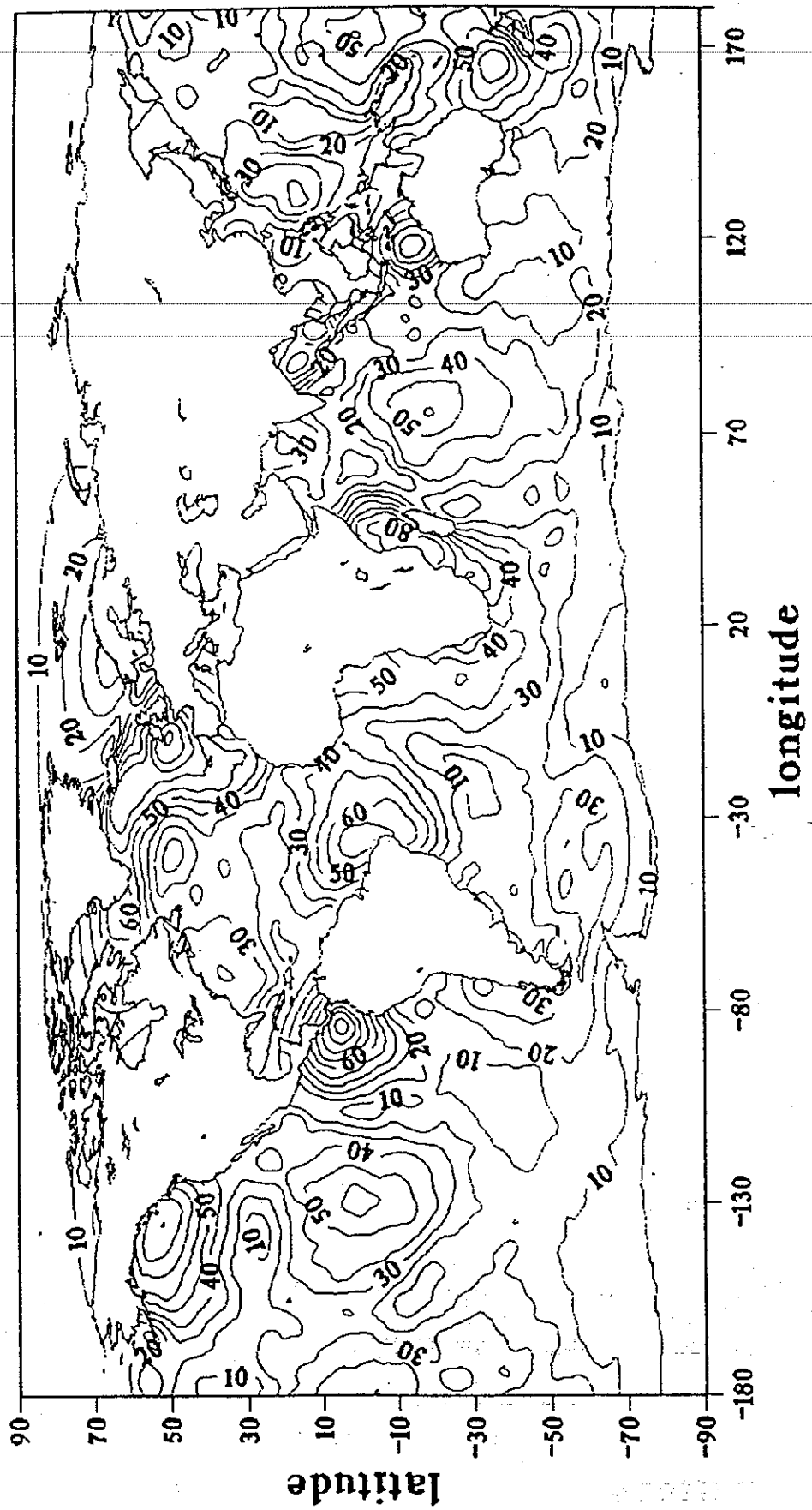

Figure 26: OMP0 model of the M_2 tide obtained by averaging 22 separate inverse solutions of 12,000 Geosat altimeter data. Amplitude in cm.

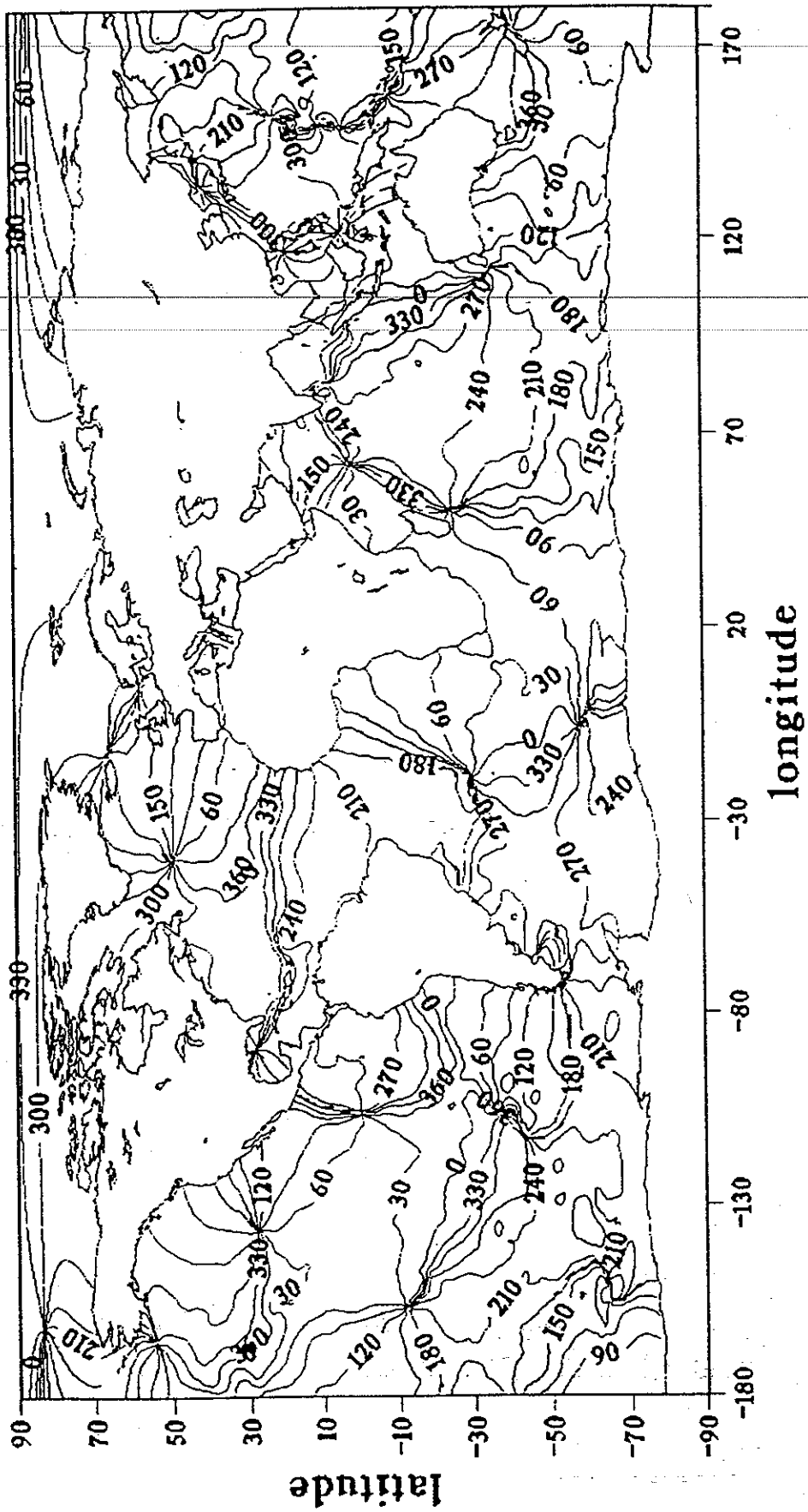

Figure 27: OMP0 model of the M_2 tide obtained by averaging 22 separate inverse solutions of 12,000 Geosat altimeter data. Greenwich phase in degrees.

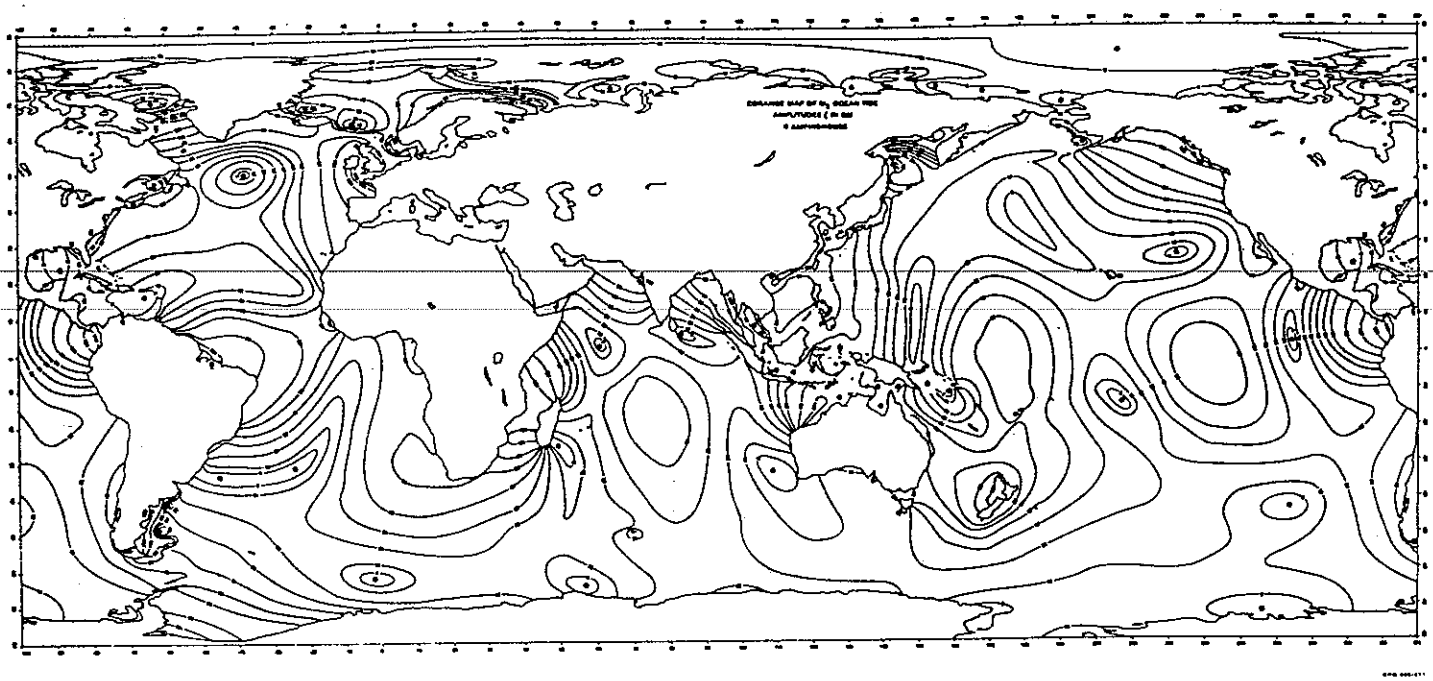

Figure 28a: Schwiderski's model of the M_2 tide. Amplitude in mm.

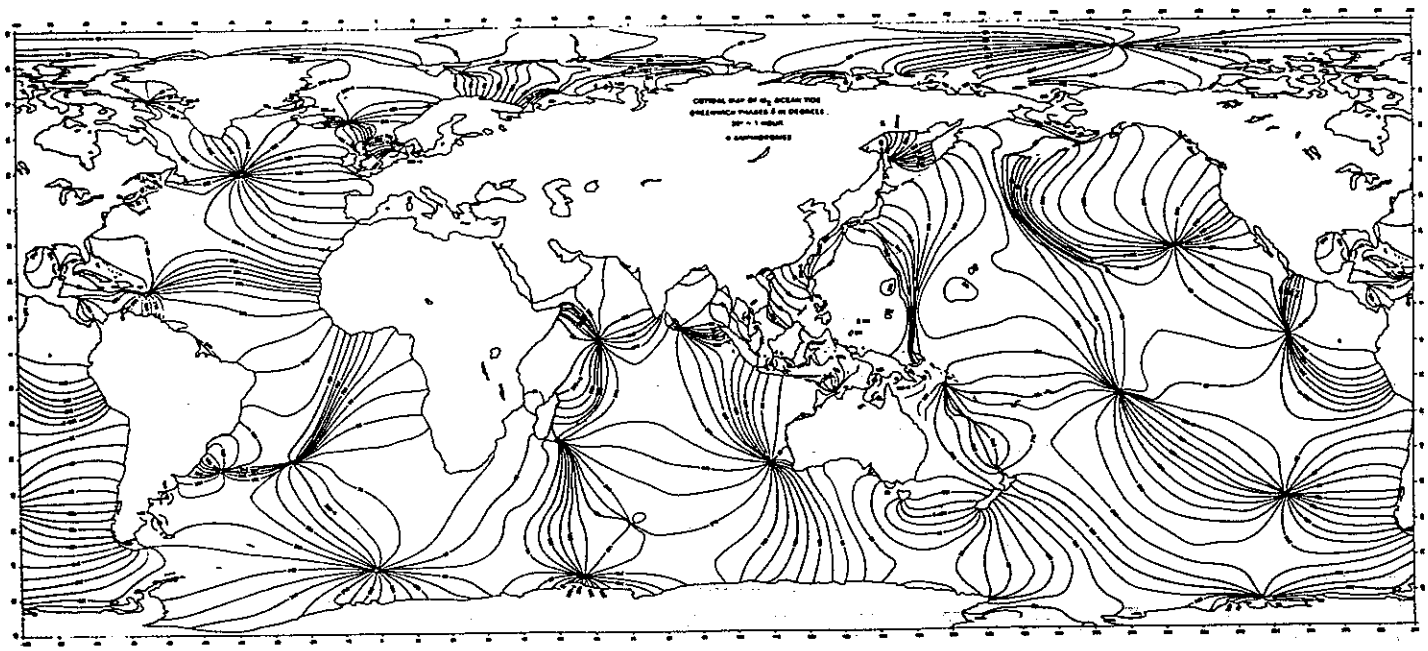

Figure 28b: Schwiderski's model of the M_2 tide. Greenwich phase in degrees.

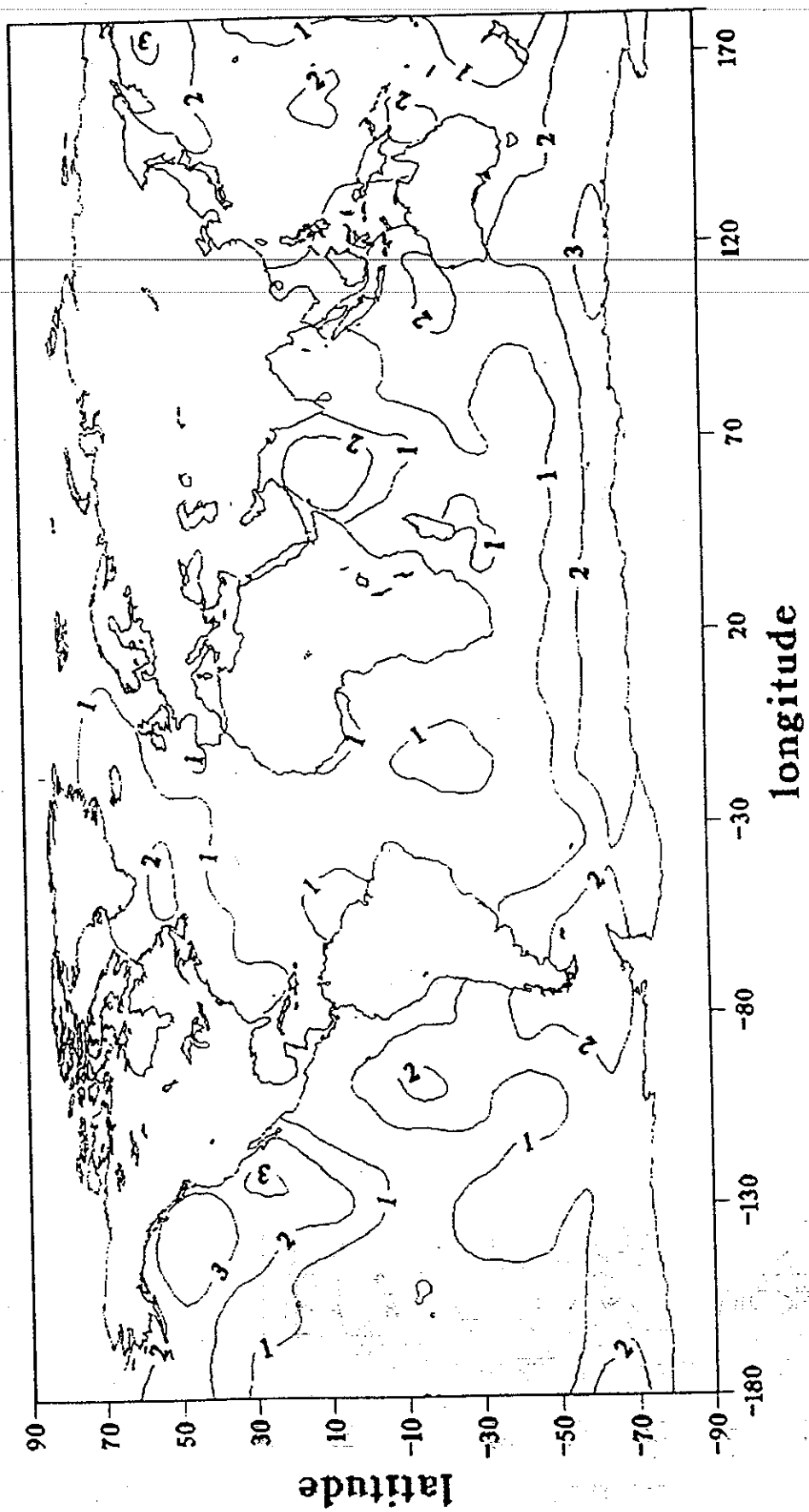

Figure 29: OMP0 model of the Q_1 tide obtained by averaging 22 separate inverse solutions of 12,000 Geosat altimeter data. Amplitude in cm.

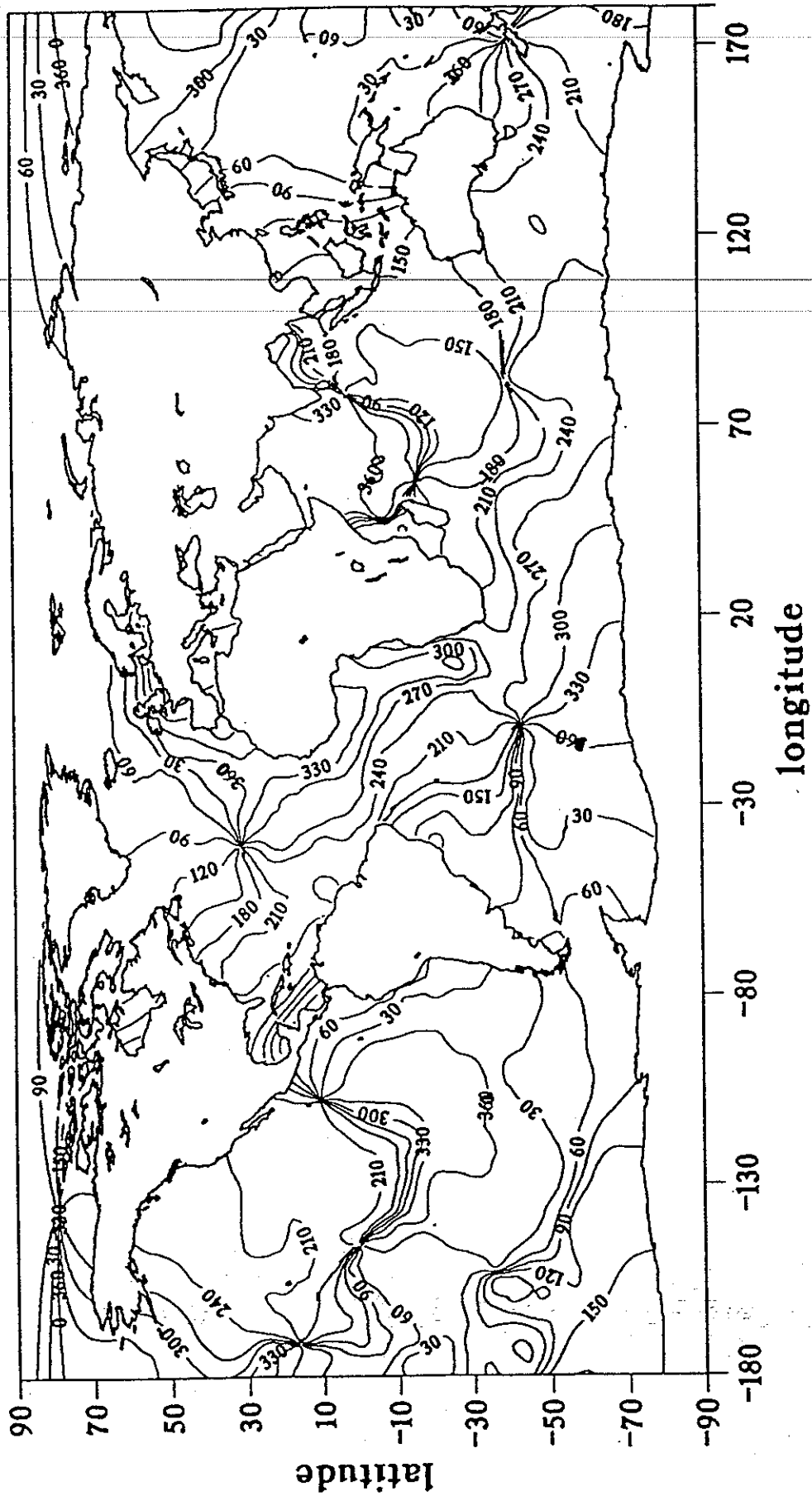

Figure 30: OMP0 model of the Q_1 tide obtained by averaging 22 separate inverse solutions of 12,000 Geosat altimeter data. Greenwich phase in degrees.

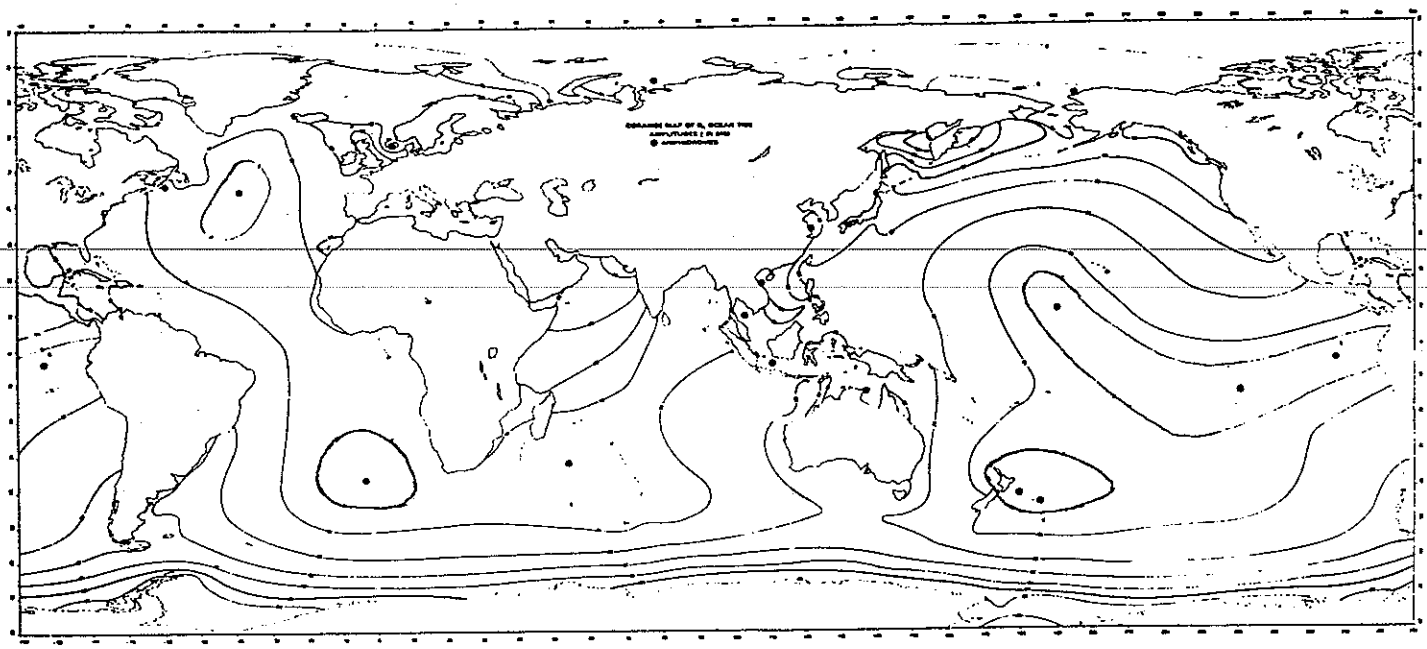

Figure 31a : Schwiderski's model of the Q_1 tide. Amplitude in mm.

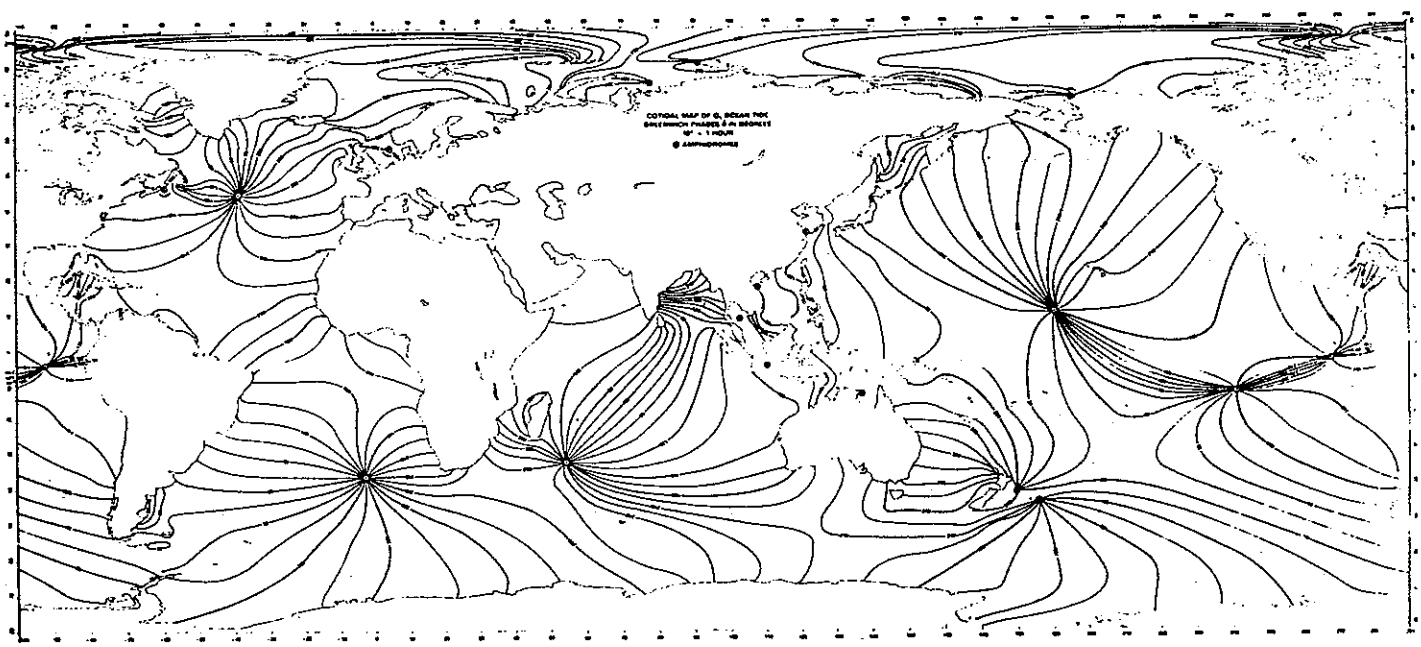

Figure 31b: Schwiderski's model of the Q_1 tide. Greenwich phase in degrees.

method; and the nodal corrections for tides were not applied. Globally, 50 hours of time CPU on a Cray2 were consumed.

The solutions are unsatisfactory along the coasts. This is not surprising because of the absence of tide gauge data supplying the poor coverage of the altimeter data in the coastal area.

Some lessons can be drawn from this first experiment. A realistic solution was obtained from the average of 22 separate solutions which are very noisy. It proves that the final accuracy of the solution depends on the number of data used. Secondly, coastal tide gauge data are absolutely needed in complement to altimeter data.

Some tests have been already conducted in order to improve the individual solutions. It appears that the covariance matrix of the radial orbit error plays a predominant role. The chosen stationary covariance was found to be not unsuited to represent the complexity of the actual orbit error. We decided to correct the altimeter data by the complex demodulation method prior to the inversion. The individual inverse tidal solutions were considerably improved. The introduction of non-stationary tidal covariance taken into account the particular dynamic in the shallow water areas leads to better solution in these areas. Last but not least, the algorithm permits now to jointly inverse tide gauge and altimeter data. Figure 32 shows a solution with a limited data set.

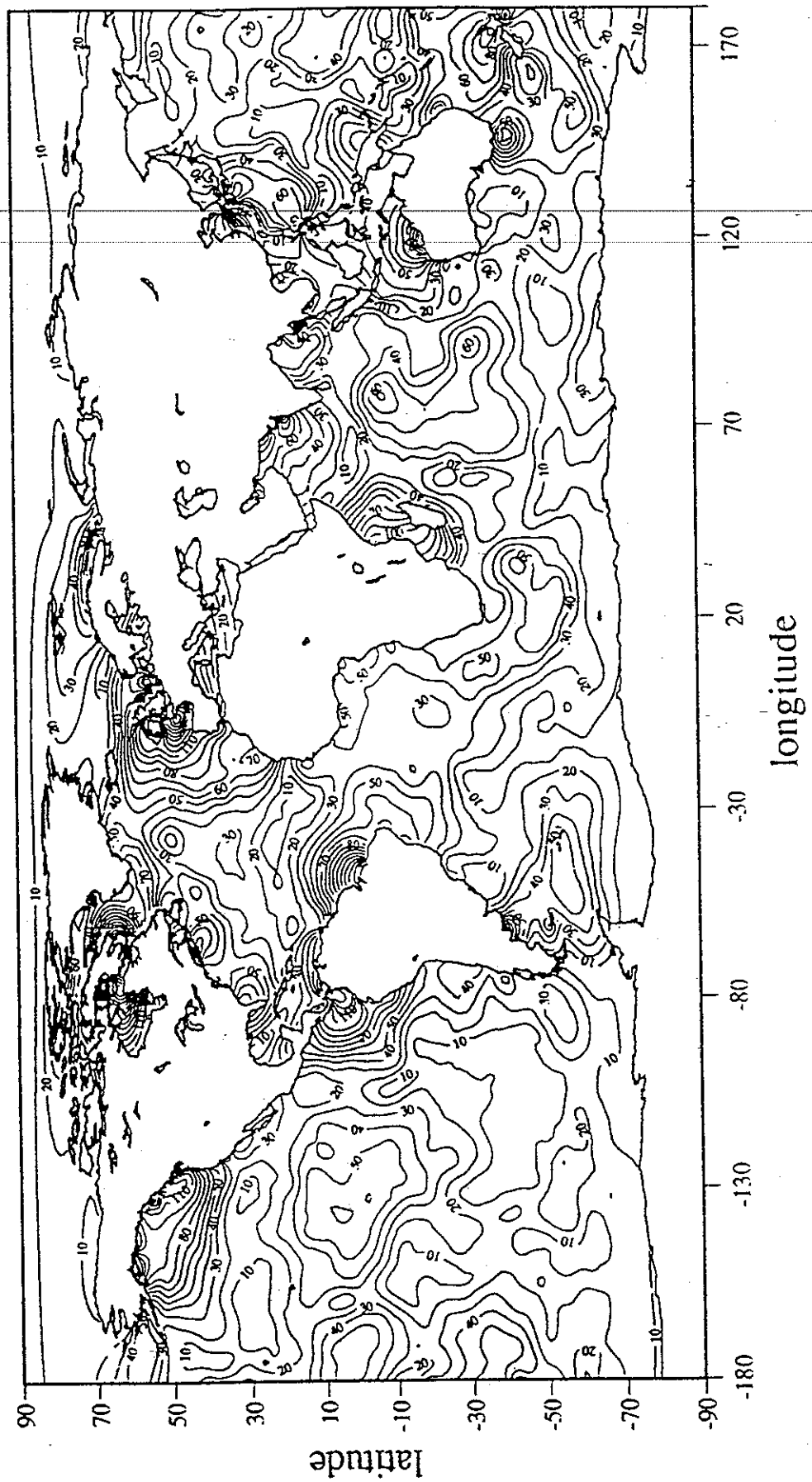

Figure 32: M_2 ocean tide solution obtained by inverting 6,000 Geosat altimeter data and tide gauge data from 400 stations.

7. Prospect

The inverse algorithm and the altimeter data are now ready to produce the best possible model which will be called OMP1 model. It will be computed from 88 data sets involving 500,000 Geosat altimeter data and 650 tide gauge data (i.e. ± 5,000 data). The altimeter data will be corrected for the radial orbit error by using the complex demodulation method. A non-stationary covariance for the ocean tide signal will be used. An other stationary covariance for the residuals of the orbit error having long spatial scale will be introduced. The OMP1 model will contain : global ocean tides charts for the principal constituents (M_2, N_2, S_2, K_2, P_1, O_1, K_1, Q_1, M_m, M_f, S_{sa}) and a global chart of the mean sea surface. All these charts will have a resolution of 0.5°x0.5°.

Residuals of all the Geosat altimeter data for one year will be computed using the a posteriori radial orbit error, the tidal and mean sea surface solutions. Further analyses of these residuals will permit :

- to estimate the short wavelengths of the mean sea surface.
- to produce maps of monthly oceanic variability.
- to inverse large data set to compute tidal solution and to improve the mean sea surface solution in marginal seas.
- to calculate global charts of ocean tides loading effects with the new model with a resolution of 0.5°x0.5° (Francis and Mazzega, 1990b).

8. References

Bloomfield, P., 1976. *Fourier Analysis of Times Series: An Introduction*, Wiley, New York.

Francis, O. and Bergé, M. 1992. Estimate of the radial orbit error by complex demodulation, *submitted to Journal of Geophysical Research.*.

Francis, O. and Mazzega, P., 1990a. M_2 world ocean tide from tide gauge and gravity loading measurements, *Cahiers du Centre Européen de Géodésie et de Séismologie*, vol. 2, 187-196.

Francis, O. and Mazzega, P., 1990b. Global charts of ocean loading effects, *J. Geophys. Res.*, 95, 11411-11424.

Francis, O. and Mazzega, P., 1991. M_2 world ocean tide from tide gauge measurements, *Geophysical Research Lett.ers*, 18, 1167-1170.

Houry S., Minster J.F., Brossier C., Dominh K., Gennero M.C., Cazenave A., Vincent P., 1992. Radial orbit error reduction and marine geoid computation from the Geosat altimeter data, *submitted to Journal of Geophysical Research.*.

Jourdin, F., Francis, O., Vincent, P. and Mazzega, P., 1991. Some results of heterogeneous inversions for ocean tides, *Journal Geophysical Research*, 20,267-20,288.

Laudet, P., 1988. Détermination du Périodogramme d'un jeu de données non équidistantes. Application à l'orbitographie, *Rapport Interne Centre National d'Etudes Spatiales*, 88/CT/DTI/MS/MO/252, Toulouse, France.

Marty, J.C., 1990. Contribution à l'étude des marées océaniques par hydrodynamique et altimétrie, *Contract CNES/CNRS*, Marché n°879, CNES 89 600400.

Mazzega, P. and Houry, S., 1989. An experiment to invert Seasat altimetry for the Mediterranean and Black Sea mean sea surface, *Geophys. J.*, 96, 259-272.

Mazzega, P. and Jourdin, F., 1991. Inverting SEASAT altimetry for tides in the Northeast Atlantic : preliminary results, In : *Tidal Hydrodynamics*, 569-592, ed. Parker, B., John Wiley, New York.

Scargle, J. D., 1982. Studies in astronomical time series analysis. II. Statistcal aspects of spectral analysis of unevenly spaced data, *The Astrophysical Journal*, 263, 835-853.

Schwiderski, E.W., Ocean Tides, I, Global tidal equations, *Mar. Geod.*, 3, 161-217, 1980a.

Schwiderski, E.W., Ocean Tides, II, A Hydrodynamic interpolation model, *Mar. Geod.*, 3, 219-255, 1980b.

Tarantola, A., 1987. *Inverse Problem Theory : Methods for Data Fitting and Model Parameter Estimation*, Elsevier, Amsterdam.